Submitted, accepted and published by :
Chemical Engineering Journal, 256 (2014) 69-84

Kinetic analysis of a Cu-based Oxygen Carrier: relevance of temperature and oxygen partial pressure on reduction and oxidation reactions rates in Chemical Looping with Oxygen Uncoupling (CLOU)

I. Adánez-Rubio, P. Gayán*, A. Abad, F. García-Labiano, L. F. de Diego, J. Adánez

Instituto de Carboquímica (ICB-CSIC), Miguel Luesma Castán 4, 50018-Zaragoza, Spain

**Corresponding author. Tel.: +34 976 733977; fax: +34 976 733318*

Email address: pgayan@icb.csic.es

Abstract

The kinetic of reduction of CuO to Cu_2O with N_2+O_2 mixtures and the oxidation of Cu_2O to CuO with O_2 of a Cu-based oxygen carrier for the CLOU process has been determined in a TGA. For kinetic determination, the O_2 concentrations were varied between 0 and 9 vol.% for reduction, and between 21 and 1.5 vol.% for oxidation reactions; temperature was varied between 1148 and 1273 K for the reduction and between 1123 and 1273 K for the oxidation. The oxygen carrier showed high reactivity

both in oxidation and reduction reactions. The nucleation and nuclei growth model with chemical reaction control properly described the evolution of solids conversion with time. The Langmuir-Hinshelwood model was able to describe the effect of oxygen concentration on reduction and oxidation rates. The reaction order was 0.5 for reduction and 1.2 for the oxidation. The kinetic constant activation energies were 270 $kJ \cdot mol^{-1}$ for the reduction and 32 $kJ \cdot mol^{-1}$ for the oxidation. The kinetic model was used to calculate the solids inventory needed in the fuel reactor for complete combustion of three different rank coals. It was possible to use a low oxygen carrier inventory in the fuel reactor (160 kg/MW_{th}) to supply the oxygen required to full lignite combustion. However, to reach high CO_2 capture efficiencies (≥95%), oxygen carrier inventories in fuel reactor higher than 600 kg/MW_{th} were needed with the lignite.

Keywords: CO_2 capture, chemical looping, CLOU, copper, kinetic.

1. Introduction

Chemical Looping with Oxygen Uncoupling (CLOU) was proposed by Mattisson et al. [1] as an efficient way to burn solid fuels with CO_2 capture avoiding the slow gasification step happening in the fuel reactor of a Chemical Looping Combustion (CLC) unit, which was usually required for converting carbon in char into gaseous compounds. CLOU process is based on CLC technology where the oxygen is transferred to the fuel by an oxygen carrier that circulates between two reactors; fuel and air reactors. CLOU process is based on the use of oxygen carrier materials which release gaseous oxygen and thereby allowing the solid fuel to burn with gas phase oxygen. These materials can be also regenerated at high temperatures in the air reactor.

CuO, Mn_2O_3 and Co_3O_4 have been identified as possible metal oxides with the property of release oxygen [1].

Fig. 1 shows a schematic diagram of a CLOU system. The fuel is physically mixed with the oxygen carrier in the fuel reactor. In the fuel reactor the fuel conversion is produced by different reactions. First the oxygen carrier releases oxygen according to:

$$2\ Me_xO_y \leftrightarrow 2\ Me_xO_{y-1} + O_2 \quad (1)$$

and the solid fuel begins to devolatilize producing a carbonaceous solid residue (char, mainly composed by carbon and ash) and volatile matter as gas product:

$$\text{Solid fuel} \rightarrow \text{Volatile matter} + \text{Char (C)} \quad (2)$$

Then, volatiles and char are burnt as in usual combustion with gaseous oxygen according to reactions (3) and (4):

$$\text{Volatile matter} + O_2 \rightarrow CO_2 + H_2O \quad (3)$$

$$\text{Char (C)} + O_2 \rightarrow CO_2 + \text{ash} \quad (4)$$

After steam condensation, a pure CO_2 stream is obtained from the fuel reactor. The reduced oxygen carrier is transported to the air reactor, where the oxygen carrier is regenerated to the initial oxidation stage with the oxygen of the air to be ready for a new cycle. Ideally, the exit stream of the air reactor contains only N_2 and unreacted O_2. The heat release over the fuel and air reactors is the same as for conventional combustion. Therefore CLOU process has a low energy penalty for CO_2 separation and low CO_2 capture costs are expected.

Up to date, several materials have been proposed to be used as oxygen carriers in the CLOU process. Cu-based [2-4] and Mn-based materials mixed with Ca, Mg, Cu, Ni, Fe or Si [5] have focused great attention. Adánez et al. [6] and Mattisson [7] summarize the

oxygen carrier developed for CLOU and the facilities where have been tested. However, the proof of the concept of CLOU process burning coal in a continuous unit has been only demonstrated with a Cu-based oxygen carrier [8]. This oxygen carrier, consists of 60 wt.% of CuO and 40 wt.% $MgAl_2O_4$ prepared by spray drying [8, 9], and it was named as Cu60MgAl. The effect of the coal rank was also analysed [10] in the CLOU unit using one anthracite, two bituminous coals, a lignite with high sulphur content [11] and biomass [12]. Complete combustion using a solids inventory in the fuel reactor of 235 kg/MW_{th} was reached. In conjunction, values close to 100 % of carbon capture efficiency were obtained at 1233 K with reactive coals and biomass. In all cases, the oxygen carrier particles showed good behaviour, as reactivity was unchanged and agglomeration problems did not occur.

For the design of the air and fuel reactors of a CLOU unit it is necessary to know the kinetic of oxidation and reduction rates of the oxygen carrier together with the kinetic of coal combustion reactions in the operation window for CLOU process. Previous kinetic studies of Cu-based oxygen carriers were mainly carried out in the window of CLC conditions, in a range of temperature between 723 to 1073 K [13]. This temperature interval is lower than that needed in CLOU process. The main difference between the CLC and the CLOU process is that in CLOU process the oxygen carrier reduction is from CuO to Cu_2O. This reaction is favoured at high temperatures as can be seen with the equilibrium diagram in Fig. 2, being the oxygen concentration at equilibrium a function of the temperature as:

$$C_{O_2,eq} = \frac{101325}{R_g T} K_{eq} = \frac{101325}{R_g T} \exp\left(22 - 2.993 \cdot 10^4 T^{-1} - 1.048 \cdot 10^6 T^{-2}\right) \quad (5)$$

Thermodynamic equilibrium set the temperatures and oxygen concentrations suitable for the CLOU process. So, the oxygen concentration at equilibrium conditions must be

high enough to allow the O_2 release in the fuel reactor and also the combustion of the fuel at the fuel reactor temperature. Moreover, the oxygen carrier must be able to oxidize by oxygen in the air reactor, but the oxygen concentration should be as low as possible in order to maximize the oxygen utilization. For example, with Cu-based materials the temperatures should be between 1173 to 1223 K in both reactors [8, 10] corresponding to oxygen concentration values at equilibrium conditions of 1.4 and 4.2 vol.%, respectively.

At high temperature and in an atmosphere with oxygen concentration lower than the equilibrium, the CuO is reduced to Cu_2O generating gaseous oxygen. This fact makes that the oxygen concentration at equilibrium a thermodynamic restriction in the reduction reaction affecting to the reduction rate. Thus, the oxygen concentration must be in a range from 0 to the oxygen equilibrium concentration in the fuel reactor. Furthermore, in the CLOU process the reduction stops at Cu_2O instead of at Cu, allowing to work at higher temperatures in CLOU than in CLC without the risk of oxygen carrier agglomeration by melting (T_{fusion} = 1508 K for Cu_2O and 1357 K for Cu). Oxidation would be carried out at the air reactor in an oxygen concentration range between 21 vol.% O_2 and the oxygen equilibrium concentration.

There are some studies on the reduction, or oxygen uncoupling, and oxidation kinetic for Cu-based materials. Table 1 shows a resume of the main kinetic parameters studied in the literature for CLOU or similar processes for the reduction and oxidation reactions; also the oxygen carrier (CuO content, support and preparation method) and the model used were shown. Most of the works were focused on the evaluation of the effect of temperature on reaction rate, thus calculating the activation energy of the process. Two types of reaction rate equations have been used to represent the CuO oxygen uncoupling and Cu_2O oxidation reaction for the CLOU process [14, 15]:

$$\left(-r_{\mathrm{Red}}\right)_{OC} = k_1 \cdot f\left(X\right) \tag{6}$$

$$\left(-r_{\mathrm{Red}}\right)_{OC} = k_2 \cdot \left(C_{O_2,eq} - C_{O_2}\right)^{n'} \cdot f\left(X\right) \tag{7}$$

It can be seen that in Eq. (6) the reduction rate only depends on temperature (included in the kinetic constant) and on oxygen carrier conversion, f(X). On the other hand, reaction rate also depends on the oxygen concentration in Eq. (7). Different values for the activation energy were obtained either Eq. (6) or Eq. (7) was considered. Thus, a global activation energy (E_1) for k_1 in Eq. (6) was calculated when the effect of temperature on both the chemical reaction barrier and the thermodynamic barrier was considered. But the kinetic activation energy was calculated for k_2 in Eq. (7), which separates the thermodynamic barrier (E_{th}) from the chemical reaction barrier (E_2).

Eqs. (6) and (7) are also valid for the oxidation reaction considering the oxidation reaction rate, $\left(r_{Ox}\right)_{OC}$, can be calculated by $\left(r_{Ox}\right)_{OC} = \left(-1\right)^{n'}\left(-r_{\mathrm{Red}}\right)_{OC}$. If the reaction order is n' ≈ 1, the global activation energy for k_1 can be calculated approximately as $E_1 \simeq E_2 + \mathrm{E_{th}}$, being $E_{th} = 255 \cdot 10^3$ J/mol in Eq. (5). It can be seen that different values for the activation energy were obtained either Eq. (6) or Eq. (7) was considered. Thus, a global activation energy (E_1) for k_1 in Eq. (6) was calculated when the effect of temperature on both the chemical reaction barrier and the thermodynamic barrier was considered jointly. But kinetic activation energy due to chemical reaction barrier (E_2) calculated for k_2 in Eq. (7) was decoupled from the thermodynamic barrier (E_{th}) considered by the oxygen concentration at equilibrium condition.

Respect to the reduction, Chadda et al. [16] did an analysis of the copper oxide capacity of storage chemical energy for a process similar to CLOU. They studied the same reaction of decomposition of CuO in a range of temperatures from 1033 to 1183 K. In this work, a global activation energy of 313 kJ/mol for the decomposition reaction was

found. Eyring et al. [17] studied the reduction kinetic for a pure CuO oxygen carrier in a TGA. They obtained a value of the activation energy for the reduction of 327 kJ/mol using an empirical first order reaction, developed for their purposes of modelling.

Similar results were found by Clayton and Whitty [15]. They determined in a TGA the reduction kinetic rate for two different Cu-based oxygen carriers: 50 wt.%CuO/TiO_2 and 45 wt.% CuO/ZrO_2, prepared by mechanical mixing and freeze granulation respectively. The global activation energies determined were 284 kJ/mol (CuO/TiO_2) and 264 kJ/mol (CuO/ZrO_2). These values were slightly lower than the values obtained by Chadda et al. [16, 17] or Eyring et al. [16, 17], but they were still high when compared to results from others.

Song et al. [18] studied in a TGA the kinetic of a Cu-based oxygen carrier with 18 wt.% of CuO supported on SiO_2, prepared by impregnation for the Chemical Looping Air Separation (CLAS) process, which uses the same oxygen uncoupling property of some metal oxides to separate oxygen from air. They considered the best model to be the Avramie-Erofeev nucleation model (N=2) with two different zones as a function of the temperature range, for temperatures between 1073 to 1173 K the global activation energy was 315 kJ/mol and in the range 1173-1248 K they obtained a value of 176 kJ/mol. This suggests that the temperature could affect to the calculated activation energy. This behaviour was also found for a CuO (50 wt.%) oxygen carrier with TiO_2 as supporting material [19]. Thus, an activation energy of 284 kJ/mol was found in the 1073-1173 K temperature interval [15], but it was lower (180 kJ/mol) if the range of temperature was increased to 1173-1273 K [19]. The same authors reported average activation energy for a Cu-based material supported on ZrO_2 of 147 kJ/mol in the temperature interval of 1073-1273 K [19], but also a decrease in the activation energy with temperature could be seen from the Arrhenius plot they showed. Similarly,

Peterson et al. [20] prepared Cu-based oxygen carrier materials by impregnation on SiC. They obtained a value of global activation energy for an oxygen carrier with 42 wt.% of CuO in the middle interval (220 kJ/mol) when the temperature was varied from 1123 to 1223 K.

However, other authors have determined activation energy values in the lower range at the low temperature interval, and even high activation energy values in the upper temperature interval; see Table 1. The reasons for obtaining high or low activation energy values are not clear. Thus, comparing results obtained with similar materials, e.g. Cu-based oxygen carriers with copper content in the range 40-60 wt.% and using ZrO_2 as inert material, activation energy values ranged from 147 to 281 kJ/mol [14, 15, 19, 21]. Nevertheless, the global activation energy was calculated to be in the lower range in most of the works. Arjmand et al. [22] studied the kinetic in a batch fluidized bed reactor of a Cu-based oxygen carrier (40 wt.% of CuO and 60 wt.% $MgAl_2O_4$) prepared by freeze granulation. They obtained a value of the global activation energy of 139 kJ/mol using the Avrami-Erofeev model (N=2). Wang et al. [21] studied the reduction reaction kinetic using three Cu-based oxygen carrier with 60 wt.% of CuO and 40 wt.% of three different supports (ZrO_2, TiO_2 and SiO_2) for CLAS process. The oxygen carriers were prepared by mechanical mixing and tested in a TGA. They obtained a value of the global activation energy of 153 kJ/mol (CuO/ZrO_2), 155 kJ/mol (CuO/TiO_2) and 145 kJ/mol (CuO/SiO_2) and they proposed to use the Avrami-Erofeev model (N=3). Similar global activation energy value of 170 kJ/mol was found for a CuO/SiO_2 material by Whitty and Clayton [19].

Also, the equipment used for reactivity investigation seems to be of low relevance. For example, Whitty and Clayton [19] studied the effect of the temperature in the reduction of three Cu-based oxygen carriers: 20 wt.% CuO/SiO_2, 50 wt.%CuO/TiO_2 and 55 wt.%

CuO/ZrO_2, prepared by incipient wetness, mechanical mixing and freeze granulation, respectively. They tested the oxygen carriers in 3 different reactor types (TGA, fluidized bed reactor and fixed bed reactor) obtaining similar results with the three facilities.

If the kinetic and the thermodynamically barriers were separated, lower values of the kinetic activation energies were determined, as result of including the temperature effect on the thermodynamic barrier; see Eq. (7). Thus, the following values for the kinetic activation energy has been reported: 58 kJ/mol [15] for CuO/TiO_2, and 67 kJ/mol [15] or 20 kJ/mol [14] for CuO/ZrO_2.

Moreover, Clayton and Whitty [15] studied the reaction order with respect to the oxygen partial pressure; they observed that the reaction rate decreased as the driving force decreased, and with an unexpected great decrease when the oxygen partial pressure was near the equilibrium pressure. However, only experiments far from the O_2 equilibrium were considered to obtain a reaction order of 1. Sahir et al. [14] calculated the reaction order with respect to CuO and obtained a value of 0.

Respect to the oxidation rate, Chadda et al. [16] did an analysis of the capacity of chemical energy storage with copper materials during the oxidation of Cu_2O in a range of temperatures form 673-773 K. In this work, an activation energy value of 76.5 kJ/mol for oxidation was found. Zhu et al. [23] reviewed the oxidation rate of a Cu plate of very high purity in a high range of temperatures from 623K to 1323 K, for metallurgic purposes. They conclude that at high temperatures (> 1173 K, typical for CLOU operation) lattice diffusion controlled the copper oxidation, and the activation energy were between 173 to 98 kJ/mol as a function of the formation of a double- or single-layer respectively.

Also, some works have studied the kinetic behaviour during oxidation of Cu_2O for CLC. Peterson et al. [20] observed that the oxidation rate decreased somewhat when the

temperature increases, due to the decrease of the driving force, i.e. the difference $\left(C_{O_2} - C_{O_2,eq}\right)$. Whitty and Clayton [19] obtained an activation energy of 202 kJ/mol in the temperature interval of 1123-1273 K when the driving force was maintained constant, which suggests that the activation energy of the thermodynamic barrier is some higher than the kinetic activation energy. The activation energy calculated by Whitty and Clayton [19] was higher than the values obtained by Zhu et al. [23]. They blame this higher apparent activation energy due to the presence of defects in the material that inhibits the lateral grown of the CuO grains [23]. Finally, Song et al. [18] studied the oxidation of different Cu-based oxygen carriers prepared by dry impregnation for CLAS (18, 29 and 48 wt.% of CuO). They evaluated the effect of the temperature in the oxidation rate, obtaining two different zones respect to the activation energy: in the range of 1073-1173 K the activation energy is positive with a value of 3 kJ/mol, but at temperatures in the 1173-1248 K interval the value of the activation energy is -43 kJ/mol. They considered that the negative value is due to both the thermodynamic barriers of the Cu_2O oxidation and the high diffusional barrier caused by the sintering effects at high temperatures [18, 23]. Also, they considered that the best model to describe the oxidation rate is a Boundary reaction model. Using this model they analysed the effect of the oxygen partial pressure during the oxidation and they obtained a reaction order for the oxygen partial pressure of 0.5. However, they use O_2 partial pressures far from the equilibrium partial pressure. Whitty and Clayton, [19] observed the oxidation rate decreased when the O_2 concentration decreased, but lower than they expected when the O_2 concentration approached to equilibrium. Chuang et al. [24] studied the oxidation kinetic with a CuO/Al_2O_3 oxygen carrier prepared by co-precipitation in a fluidized bed reactor. They studied the reaction order for the oxygen concentration and they observed that the order varied with the O_2 concentration. They

explain that this behaviour is typical when the reaction rate is controlled by a Langmuir-Hinshelwood mechanism.

As a conclusion, very disperse values for the kinetic data of Cu-based materials for CLOU were found. These data were found from studies analyzing only temperature dependency or oxygen concentration but far away from equilibrium conditions. For these reasons, it is necessary to analyze the effect of temperature and oxygen concentration on oxidation and reduction reactions in a broad range of operation values.

The aim of this work was to determine the kinetic of reduction in N_2-O_2 mixtures and oxidation reactions with O_2 of a Cu-based oxygen carrier (Cu60MgAl) prepared by spray drying in the range of operation of the CLOU process. This material has been previously used to successfully prove the CLOU concept with several solid fuels. The effect of O_2 concentration and temperature was investigated both for oxygen uncoupling and oxidation processes in TGA. The kinetic parameters obtained were used to determine the solids inventories needed in a CLOU system working with this Cu-based oxygen carrier. Kinetic parameters obtained in this work can be implemented in a design and optimization tool for CLOU process.

2. Experimental

2.1. The Cu-based oxygen carrier

The oxygen carrier used in this work was a Cu-based material prepared by spray drying. Oxygen carrier particles were manufactured by VITO (Flemish Institute for Technological Research, Belgium) using CuO (Panreac, PRS) and $MgAl_2O_4$ spinel (Baikowski, S30CR) as raw materials. The particles were calcined 24 h at 1373 K. The CuO content was 60 wt.%. The particle size of the oxygen carrier was +0.1-0.3 mm.

From now on, the oxygen carrier is named as Cu60MgAl. Table 2 shows the main properties of this material, which were presented in previous works [2, 8-11, 25].

The oxygen transport capacity, R_{OC}, is an important characteristic of the oxygen carrier. R_{OC} has relevance on the solids circulation rate and solids inventory in a CLC unit [26]. R_{OC} was calculated in TGA in nitrogen atmosphere as $R_{OC} = (m_{Ox}-m_{Red})/m_{Ox}$, being m_{Ox} the mass of fully oxidized particles and m_{Red} in the reduced form after oxygen uncoupling, i.e. when all CuO has been reduced to Cu_2O.

Preliminary results showed that this material has adequate values of reactivity and oxygen transport capacity in fluidized-bed conditions [9, 25]. High combustion rates with complete combustion to CO_2 and H_2O were obtained with this material using a low solids inventory in the fuel reactor of a CLOU unit burning different types of coal and biomass [8, 10].

2.2. Experimental set-up

Multicycle tests to analyze the reactivity of the oxygen carrier during successive reduction-oxidation cycles were carried out in a TGA CI Electronics type described elsewhere [2]. The desired mass of oxygen carrier was loaded in a platinum wired mesh basket (14 mm diameter and 8 mm height). Initially, to establish whether thermodynamic limitations, external film mass transfer and/or inter-particle diffusion were affecting the reaction rate, the sample weight and the gas flow rate were varied in the range of 40 to 100 mg and from 10–40 NL/h. The composition of the gas flow were pure N_2 for the reduction and air for the oxidation. It was found that using a sample mass lower than 70 mg, the control of gas diffusion inside the particles was avoided. On the other hand, it was found that the reaction rate was not controlled by interparticle

diffusion or diffusion through the gas film around the particle when N_2 flow was higher than 20 NL/h. Therefore, gas flow rate of 25 NL/h and 50 mg of solids were used to reduce mass transfer resistance around the solid sample. As it was shown by Gayán et al., [2], the use of these conditions ensured the minimization of external film mass transfer and/or inter-particle diffusion effects in the TGA. Moreover, the temperature in the reaction zone can greatly affect to the reaction rate and it was carefully checked. Deviations lower than 2 K were found in all cases during the reaction period. Moreover, previous studies showed that oxygen carrier particles can be considered isothermal during reduction or oxidation [27].

The sample was heated to the set operating temperature in air atmosphere. After stabilization, the experiment started by exposing the oxygen carrier to alternating reducing and oxidizing conditions. The experiments were carried out at temperatures between 1123-1273 K for the reduction and oxidation reactions. These temperatures were selected as a function of the thermodynamic equilibrium of the CuO/Cu_2O system, as shown in Fig. 2, being this temperature interval of interest for fuel and air reactors in CLOU process [8, 10].

The reaction gas mixture was composed by O_2 and N_2 in different relations for the reduction and oxidation. Table 3 summarizes both temperature and oxygen concentrations used for reduction and oxidation tests. For the reduction, the amount of O_2 varied from 0 to 9 vol.%. In the case of the oxidation, the oxidation reaction was carried out after reducing the oxygen carrier in N_2 at 1273 K and the concentration of O_2 was varied between 21 to 2.5 vol.%. These conditions allowed studying the effect of the oxygen concentration far away and near the equilibrium conditions. Three cycles of reduction and oxidation were carried out for each experiment. In all cases, reaction rate

was stable during cycles. Conversion vs. time curves showed in this work corresponded to the third cycle of each experimental condition.

2.3. Data evaluation

The release of O_2 (reduction of CuO) and the oxidation of Cu_2O is given by the following equilibrium:

$$4CuO \rightleftarrows 2Cu_2O + O_2 \tag{8}$$

The oxygen carrier conversion was calculated for the reduction and oxidation as:

$$X_{Red} = \frac{m_{Ox} - m}{m_{Ox} - m_{Red}} \tag{9}$$

$$X_{Ox} = 1 - \frac{m_{Ox} - m}{m_{Ox} - m_{Red}} \tag{10}$$

being m the mass of sample at each time, m_{Ox} is the mass of the sample fully oxidized and m_{Red} is the mass of the sample in the reduced form, i.e. when copper was in the Cu_2O form.

The reaction rate for both, reduction and oxidation, are calculated from TGA conversion data using the following expressions:

$$\left(-r_{\mathrm{Red}}\right)_{OC} = R_{OC}\frac{dX_{\mathrm{Red}}}{dt} \tag{11}$$

$$\left(r_{Ox}\right)_{OC} = R_{OC}\frac{dX_{Ox}}{dt} \tag{12}$$

3. Results

To obtain the reduction and oxidation kinetic, TGA tests were carried out varying the temperature and the oxygen concentration in a wide range of values, from far away of the equilibrium to values near the equilibrium.

3.1. TGA results for oxygen uncoupling (CuO to Cu_2O)

Fig. 3(a) shows conversion versus time curves for the Cu60MgAl oxygen carrier for different temperatures between 1148 to 1273 K, using pure N_2 in the reacting environment during the reduction, and a O_2 concentration equal to 0 vol.%. It can be seen that when the temperature increases, the reduction rate increases. Considering reduction rate given by Eq. (7), reaction rate increased with temperature because the increase of the kinetic constant and the oxygen driving force. Often, this effect is expressed by means of the difference between the oxygen concentration at equilibrium and the oxygen concentration in the system surrounding of the particles, i.e. $\left(C_{O_2,eq} - C_{O_2}\right)$. Thus, the reduction rate depends on the O_2 concentration at the external surface of the particles and the O_2 concentration at equilibrium conditions, which also increases with temperature following Eq. (5).

Fig. 3(b) shows the conversion versus time curves obtained for the Cu60MgAl oxygen carrier for three different temperatures during the reduction, using a concentration of 1.5 vol.% of O_2 in N_2. It can be observed that these curves were slower than the curves at the same temperature without oxygen. This figure confirms that the reaction rate decreases when the driving force decreases due to the approaching of the O_2 concentration to the equilibrium concentration.

To analyse the effect of the oxygen concentration on the reduction rate, Fig. 4 shows conversion vs. time curves for oxygen reduction reaction of Cu60MgAl obtained for O_2

concentration values from 0 to 9 vol.% at 1273 K. This interval of O_2 concentration has been chosen due to the maximum O_2 concentration is limited by the O_2 concentration at equilibrium condition, e.g. 12 vol.% at 1273 K; so O_2 concentration during TGA test was lower than equilibrium concentration. The oxygen uncoupling rate decreases when the O_2 concentration increases due to the decrease in the driving force of the reaction. This decrease was more pronounced when the O_2 partial pressure was close to the equilibrium concentration. Moreover, it was not possible to detect a change in the mass of the sample in the TGA when the O_2 concentration was very close to the equilibrium (y_{O_2} > 9 vol.%), because the reaction rate was very slow. This behaviour was also described by Clayton and Whitty [15], during the reduction when the driving force was close to zero.

3.2. TGA results for oxidation (Cu_2O to CuO)

Fig. 5(a) shows conversion vs. time curves obtained for oxidation of Cu_2O in reduced oxygen carrier samples at oxygen concentration values from 21 to 2.5 vol.% at 1173 K. The oxidation rate was fast when the oxygen concentration was much higher than the oxygen concentration at equilibrium conditions, but quickly decreases as the oxygen concentration approach to the equilibrium concentration. This effect also was observed by Whitty and Clayton [19] when the driving force of the oxidation reaction decreased. Fig. 5(b) shows conversion vs. times curves for the Cu60MgAl oxygen carrier for different temperatures between 1123 to 1273 K, using air as reactant gas. It can be seen that reaction rate decreased when the temperature increased, being the slowest the reaction at 1273 K, due to the decrease in the driving force of the reaction, which in this case is $\left(C_{O_2} - C_{O_2,eq}\right)$. So, the oxygen driving force decreases as temperature increases due to $C_{O_2,eq}$ increases with temperature. This behaviour was observed by Zhu et al. [23]

for the oxidation of pure copper, but with an additional reason to justify their results. They considered that the decrease in the oxidation rate with the temperature was due to the high diffusional barrier caused by the sintering effects at high temperatures, additionally to the thermodynamic barriers of the Cu_2O oxidation.

3.3. Kinetic information from conversion curves

With the different conversion vs. time curves obtained for the reduction and oxidation as a function of the temperature, it was possible to obtain the evolution of the reaction rate with solids conversion. The maximum values calculated for every curve was used to obtain the global activation energy for the reduction and oxidation rates from the Arrhenius plot; see Fig. 6. The calculated value of the global activation energy for the reduction reaction was 245 kJ/mol, which is in the same order than the values obtained by Sahir et al. [14] with a oxygen carrier 40 wt.% of CuO supported by ZrO_2 (281 kJ/mol), Peterson et al. [20] for a material with 42 wt.% CuO being SiC the support (220 kJ/mol), and Clayton and Whitty [15] for two Cu-based oxygen carriers with a 50 wt.% and 45 wt.% of CuO supported on TiO_2 (284 kJ/mol) and ZrO_2 (264 kJ/mol), respectively.

Following the same procedure, a value for the apparent activation energy of -37 kJ/mol was calculated for the oxidation reaction; see Fig. 6. This value is similar to the value obtained by Song et al. [18], who calculated a negative apparent activation energy of -43 kJ/mol in the range of temperature 1173-1248 K.

Moreover, from the conversion vs. time curves obtained at different oxygen concentrations, some information can be extracted about the reaction order with respect to the oxygen concentration considering Eq. (7). Fig. 7(a) shows the curve of the

$\ln\left(-r_{Red}\right)_{OC}$ as a function of the $\ln\left(C_{O_2,eq}-C_{O_2}\right)$. Considering Eq. (7), the reaction order corresponded to the slope in Fig. 7(a). However, a constant slope can not be calculated, which means that the reaction order changed with the oxygen concentration. Considering results showed in Fig. 7(a), an expression for the effect of oxygen concentration such Eq. (7), i.e. $f(C_g)=\left(C_{O_2,eq}-C_{O_2}\right)^{n'}$, seemed to be not valid when a wide range of values of oxygen concentration was considered.

Similarly to the analysis of the reduction period, Fig. 7(b) shows the reaction rate as a function of the oxygen concentration. In this case a constant slope can be calculated. Therefore, the reaction order does not depend on the oxygen concentration, and it was found a *n'* value of 1. However, Chuang et al. [24] observed a change in the reaction order with the oxygen concentration for the oxidation of a Cu-based oxygen carrier, similarly to what we found for the reduction in this work. Chuang et al. [24] suggested that this behaviour can be explained by using a Langmuir-Hinshelwood mechanism for the Cu_2O oxidation.

Subsequently, the Langmuir-Hinshelwood mechanism was considered in this work to determine the kinetic for the reduction reaction. To be consequent with the reduction, also a Langmuir-Hinshelwood mechanistic model was used to describe the oxidation in the CLOU process. In this way, results obtained here and found by Chuang et al. [24] could be adequately predicted for the oxidation reaction.

3.4. Kinetic model

3.4.1. Reduction from CuO to Cu_2O

A surface reaction model using a Langmuir-Hinshelwood mechanism is here proposed to describe the CuO reduction reaction to Cu_2O with O_2 generation. The CuO in the surface decomposes into Cu_2O by reaction with *a* active sites giving oxygen adsorbed in the surface. Then oxygen is desorbed to O_2, regenerating the *a* active sites in the surface [28]. Applying this model to the decomposition of CuO, following equations are obtained:

1. Chemical decomposition of CuO into Cu_2O and adsorbed O_2, which is a dynamic equilibrium between forward and backward reaction:

$$4CuO + aL \underset{k_b}{\overset{k_f}{\rightleftharpoons}} 2Cu_2O + aL(O_2), \qquad K_1 = \frac{k_f}{k_b} \tag{13}$$

2. Desorption of adsorbed O_2:

$$aL(O_2) \underset{k_A}{\overset{k_D}{\rightleftharpoons}} aL + O_2, \qquad K_2 = \frac{k_D}{k_A} \tag{14}$$

$aL(O_2)$ is one molecule of O_2 chemisorbed on *a* active sites L.

When the reaction is controlled by chemical decomposition, Eq. (13), the reaction rate is given by:

$$\frac{dX_{\mathrm{Red}}}{dt} = k_{\mathrm{Red}} S_{CuO} (1-\theta) \left(1 - \frac{C_{O_2}}{C_{O_2,eq}}\right) \cdot f(X_{\mathrm{Red}}) \tag{15}$$

where θ is the fraction of actives sites occupied by O_2. At these conditions, it is possible to use different adsorption isotherms to obtain the value of θ. García-Labiano et al. [29] selected the Freundlich isotherm to properly describe the $CaCO_3$ calcination [29]. In this case, the use of the Freundlich isotherm successfully described the effect of CO_2

concentration on the $CaCO_3$ calcination rate, which showed an effect of the CO_2 concentration on the reaction rate similar to the O_2 effect observed for the reduction reaction in this work. Thus, the Freundlich isotherm was selected in this work to describe the fraction of occupied active sites, i.e. θ parameter, which was calculated by the following equation:

$$\theta = cC_{O_2}^{1/n} \tag{16}$$

$$c = c_0 e^{-E_c/R_g T} \tag{17}$$

Combining Eq. 15 and Eq. 16, the reaction rate expression is as follow:

$$\frac{dX_{\mathrm{Red}}}{dt} = k_{\mathrm{Red}} f(X_{\mathrm{Red}}) S_{CuO} \left(1 - cC_{O_2}^{1/n}\right)\left(1 - \frac{C_{O_2}}{C_{O_2,eq}}\right) \tag{18}$$

Different models have been used for the $f(X_{Red})$ function in Eq. (18), including nucleation mechanism [18, 21, 22] or first order chemical reaction [14, 16]. The Langmuir-Hinshelwood mechanism is a surface reaction model widely used for gas-solid catalytic reactions. Due to this surface reaction, in this work it was proposed using the nucleation model to describe the conversion dependency in the reaction at the grain surface of the oxygen carrier particles.

The Avrami-Erofeev [30] equation corresponding to the nucleation mechanism is the following:

$$f(X_{\mathrm{Red}}) = N^{-1}\left(1 - X_{\mathrm{Red}}\right)\left[-ln\left(1 - X_{\mathrm{Red}}\right)\right]^{1-N} \tag{19}$$

The final expression for the reduction reaction rate, including Eq. (19) for the conversion function, is the following:

$$\frac{dX_{\mathrm{Red}}}{dt} = k_{\mathrm{Red}} S_{CuO} \left(1 - cC_{O_2}^{1/n}\right)\left(1 - \frac{C_{O_2}}{C_{O_2,eq}}\right)\cdot\left(N^{-1}\left(1 - X_{\mathrm{Red}}\right)\left[-ln\left(1 - X_{\mathrm{Red}}\right)\right]^{1-N}\right) \tag{20}$$

By integration of Eq. (20), the following equation was obtained to calculate the conversion evolution with time:

$$\left[-\ln\left(1-X_{\mathrm{Red}}\right)\right]^{N}=k_{\mathrm{Red}}S_{CuO}\left(1-cC_{O_2}^{1/n}\right)\left(1-\frac{C_{O_2}}{C_{O_2,eq}}\right)t \tag{21}$$

An effective kinetic constant was defined as:

$$k'_{\mathrm{Red}}=k_{\mathrm{Red}}S_{CuO}=k'_{\mathrm{Red},0}e^{-E_{\mathrm{Red}}/R_gT} \tag{22}$$

The kinetic model has four parameters at each temperature (N, n, k'_{Red} and c), which must be calculated as a function of temperature. The value of N represent the type of nucleation and the nuclei growth in the model, which value is usually fixed between 1/4 and 3. To calculate the best value of N, Fig. 8(a) shows a plot of $\left(-\ln\left(1-X_{\mathrm{Red}}\right)\right)^{N}$ vs. time for different values of N using conversion vs. time data of Fig. 3. Linear regression of each data shows the fit to a linear plot. Table 4 shows the values of the correlation coefficients for the different values of N. Best fitting to a linear curve correspond to N equal to 3/4. This procedure has been done for the conversion data at each temperature and oxygen concentration analysed in this work, obtaining the same result of N for all of them.

To determine the values of the chemical rate constant, k'_{Red}, and its variation with temperature, experiments carried out at different temperatures between 1148 to 1273 K with an atmosphere of 100 vol.% N_2 were considered. In this case, Eq. (21) is simplified to $\left[-\ln\left(1-X_{\mathrm{Red}}\right)\right]^{N}=k'_{\mathrm{Red}}t$. Considering an Arrhenius dependence of k'_{Red}, Fig. 9 shows the Arrhenius plot for the reduction reaction, and Table 5 shows the kinetic parameters for pre-exponential factor and activation energies obtained. The value of the activation energy was 270 kJ mol^{-1}. This value can not be compared with activation energy data

from the literature because the kinetic model here proposed has not been previously used. The activation energy determined depends on the number of temperature dependent parameters considered in the kinetic model. Thus, the global activation energy was calculated with only k_1 as function of temperature, see Eq. (6). Kinetic activation energy was calculated with two temperature dependent parameters, i.e. k_2 and $C_{O_2,eq}$, see Eq. (7); in this work the activation energy had an additional parameter, c, affected by temperature in the kinetic model proposed.

Parameters n and c in Eq. (21) were calculated considering the effect of the partial pressure of oxygen in the oxygen carrier reduction rate. After integration and some algebra with Eq. (20), the following expression was obtained:

$$Y_R = \ln\left\{1 - \frac{1}{k'_{\mathrm{Red}}\left(1-\frac{C_{O_2}}{C_{O_2,eq}}\right)\left(N^{-1}\left(1-X_{\mathrm{Red}}\right)\left[-ln\left(1-X_{\mathrm{Red}}\right)\right]^{1-N}\right)}\left[\frac{\mathrm{d}X_{\mathrm{Red}}}{\mathrm{d}t}\right]_{X_{\mathrm{Red}}=0.2}\right\} = \ln(c) + \frac{1}{n}\ln\left(C_{O_2}\right) \qquad (23)$$

Reaction rate was calculated for $X_{\mathrm{Red}} = 0.2$ due to a maximum conversion rate at this X_{red} value is reached using this model with $N = 3/4$.

Plotting the left handside of Eq. (23), Y_R, parameters c and n can be calculated from the origin and slope of the plot Y_R vs. ln(C_{O_2}); see Fig. 10(a). From this, a value of 0.5 for n (see Table 5) for all temperatures was found. Different values of c were obtained at each temperature. Considering an Arrhenius dependence of c, Fig. 9 shows the Arrhenius plot for the reduction reaction, and Table 5 shows the parameters for pre-exponential factor and activation energies obtained for c from Eq. (17). It can be seen that the value of the activation energy for the parameter c is negative (-240 kJ/mol), as it corresponds to an adsorption process.

The Freundlinch isotherm and the nucleation model were used to fit experimental conversion vs. time data for different O_2 concentrations and temperatures. Fig. 3 (a) shows experimental and theoretical conversion vs. time curves at different temperatures and 0 vol.% of O_2. Fig. 3(b) shows experimental and theoretical lines of conversion vs time for three different temperatures (1223, 1248 and 1273 K) during reduction period using an O_2 concentration of 1.5%. Fig. 4 shows a comparison between experimental data and model predictions for different O_2 concentrations at constant temperature. It can be seen a very good fit between experimental and theoretical curves with the proposed kinetic model for all the temperature and oxygen concentration intervals, including reaction conditions with O_2 concentration far away and close to the equilibrium. This result indicates that the Freundlinch isotherm with a nucleation model with $N = 3/4$ was valid to describe the decomposition of the CuO in a broad range of O_2 concentrations. Thus, the kinetic model here proposed properly prediced the reaction rates when the O_2 concentrations was close to the equilibrium, where previous literature models had failed [15]. This condition is required in the fuel reactor of a CLOU unit to avoid unconverted compounds exiting the fuel reactor [8, 25].

3.4.2. Oxidation from Cu_2O to CuO

Also, a Langmuir-Hinshelwood mechanistic model has been used to describe the chemical reaction of Cu_2O oxidation in the CLOU process.

1. Adsorption of O_2 over the surface of Cu_2O:

$$O_2 + aL \underset{k_D}{\overset{k_A}{\rightleftharpoons}} aL(O_2) \qquad K_3 = \frac{k_A}{k_D} \tag{24}$$

2. Chemical reaction of Cu_2O oxidation to give CuO:

$$2Cu_2O + aL(O_2) \underset{k_f}{\overset{k_b}{\rightleftharpoons}} 4CuO + aL \qquad K_4 = \frac{k_b}{k_f} \tag{25}$$

When the reaction is controlled by the surface chemical reaction, Eq. (25), the reaction rate is given by:

$$\frac{\mathrm{d}X_{Ox}}{\mathrm{d}t} = k_{Ox} S_{Cu_2O} c C_{O_2}^{1/n} \left(1 - \frac{C_{O_2,eq}}{C_{O_2}}\right) f(X_{Ox}) \tag{26}$$

Similar to the reduction analysis, value of θ was calculated with Freundlich isotherm, i.e. Eq. (16). The nucleation model was also considered for the oxidation reaction. The expression for the oxidation reaction rate, including the conversion evolution function, is the following:

$$\frac{dX_{Ox}}{dt} = k_{Ox} S_{Cu_2O} \cdot c C_{O_2}^{1/n} \left(1 - \frac{C_{O_2,eq}}{C_{O_2}}\right) \cdot \left(N^{-1}(1 - X_{Ox})\left[-ln(1 - X_{Ox})\right]^{1-N}\right) \tag{27}$$

Integrating Eq. (27) the following expression was obtained to calculate the conversion evolution with time:

$$\left[-\ln(1 - X_{Ox})\right]^N = k_{Ox} S_{Cu_2O} c C_{O_2}^{1/n} \left(1 - \frac{C_{O_2,eq}}{C_{O_2}}\right) t \tag{28}$$

Parameters k_{Ox} and c could not be calculated separately for oxidation reaction. In this case, an effective kinetic constant for oxidation reaction was defined as:

$$k'_{Ox} = k_{Ox} S_{Cu_2O} c = k'_{Ox,0} e^{-E_{Ox}/R_g T} \tag{29}$$

Thus, it is necessary to determine three parameters for each temperature: N, n and k'_{Ox}. To know the best value of N, Fig. 8(b) shows a plot of $\left(-\ln(1 - X_{Ox})\right)^N$ vs. time for different values of N. Linear regression of each data show the fit to a linear plot. Table 4 shows the values of the correlation coefficients for the different values of N. Best fitting

correspond to N equal to 3/4. This procedure has been done for the conversion data obtained at each temperature analyzed in this work, obtaining the same result of N for all of them.

Parameters n and $k_O^{'}$ for the oxidation reaction were obtained from a plot of Y_{Ox} vs. $\ln\left(C_{O_2}\right)$ at 1173 K, as it was described by the following equation derived from Eqs. (27) and (29), for X_{Ox} = 0.2.

$$Y_{Ox} = \ln\left\{\frac{1}{\left(1-\frac{C_{O_2,eq}}{C_{O_2}}\right)\left(N^{-1}\left(1-X_{Ox}\right)\left[-ln\left(1-X_{Ox}\right)\right]^{1-N}\right)}\left[\frac{\mathrm{d}X_{Ox}}{\mathrm{d}t}\right]_{X_{Ox}=0.2}\right\} = \ln\left(k_{Ox}^{'}\right)+\frac{1}{n}\ln\left(C_{O_2}\right) \qquad (30)$$

Fig. 10(b) shows the plot and the linear regression of Y_{Ox} vs. $\ln\left(C_{O_2}\right)$. A value of n equal to 1.2 was obtained. Experiments at different temperatures between 1123 and 1273 K and 21 vol.% O_2 were considered to calculate the temperature dependence of the kinetic constant. Considering an Arrhenius dependence of $k_{Ox}^{'}$, pre-exponential factor and activation energy can be obtained. Fig. 9 shows the Arrhenius plot for the oxidation reaction, and Table 5 shows the kinetic parameters for pre-exponential factor and activation energy obtained. An activation energy of 32 kJ mol^{-1} was obtained in this work for the oxidation kinetic constant.

Finally, Fig. 5(a) shows experimental and theoretical conversion vs. time curves obtained for different O_2 concentrations. It can be seen that there was a good agreement between the experimental and predicted data by the kinetic model with the Freundlinch isotherm. The predictions were good in all the range of O_2 concentrations used. This result indicates that the kinetic model with Freundlinch isotherm was valid to describe the oxidation of the Cu_2O in a broad range of O_2 concentrations, even at concentrations very close to the equilibrium conditions. On the other hand, Fig. 5(b) shows

experimental and theoretical conversion vs. time curves at different temperatures. It can be seen that a very good fitting was obtained with the nucleation model.

We can conclude that with the kinetic model developed in this work, it is possible to predict the reduction and oxidation reaction rates at different oxygen concentrations and different temperatures in a broad range of operation conditions suitable for the CLOU operation process.

4. Simulation of the CLOU process with kinetic data

In order to design a CLOU system, the most important parameters are the solids inventory in the system and the oxygen carrier circulation rate. Both parameters are highly influenced by the material reactivity and its oxygen transport capacity. With the kinetic data determined in this work, the CLOU process was simulated by determining the carbon capture efficiency for different coals as a function of solids inventory and solids circulation rate.

4.1. Solids inventory and solids circulation rate to transfer oxygen from air to fuel

The solids circulation rate was calculated by an oxygen mass balance in the system. A simplified model was developed by the authors [26] and later modified for the *i*G-CLC process [31] for the use of solid fuels. The circulation rate of solids per MW_{th}, $\dot{m}_{OC}$, that depends on the composition and heat value of the solid fuel, can be calculated as:

$$\dot{m}_{OC} = \frac{10^3 m_O}{LHV \cdot R_{OC} \cdot \Delta X_{OC}} \quad (31)$$

m_O being the mass of oxygen required per kg of solid fuel to full combustion, as for the case of the conventional combustion with air, LHV the lower heating value of the solid fuel and ΔX_{OC} the variation of the oxygen carrier conversion in every reactor.

The circulation rate of solids between both reactors was calculated as a function of the variation of the oxygen carrier conversion and it was shown in Fig. 11 when a lignite is used, with a corresponding m_O = 1.2 kg oxygen per kg of coal and a LHV of 16250 kJ/mol. The circulation rate is higher at low values of ΔX_{OC}, and decreases quickly when the conversion variation of the oxygen carrier at the fuel reactor increases, reaching low values when the conversion is near to 1. Abad et al. [26] estimated the maximum circulation rate feasible in a CLC plant without increased costs and with commercial experience to be 16 kg s^{-1} per MW_{th}. This means that the minimum value of ΔX_{OC} must be 0.1 and it is necessary to operate at higher values.

The minimum mass of solids in the fuel and air reactors per MW_{th} of fuel, m_{OC}, for the combustion of solid fuels was calculated by doing a mass balance to the fuel reactor [31]:

$$m_{OC} = \frac{10^3 m_O}{LHV \cdot R_{OC} \left(\overline{\frac{dX_i}{dt}} \right)} \qquad (32)$$

The average reactivity for each reactor was obtained considering the average gas concentration in the reactor and the solids residence time distribution in the reactor as perfect mixing.

Different average oxygen concentration was assumed either in fuel or air reactor. In a CLOU process, the minimum solids inventory in the fuel reactor to transfer the required oxygen for fuel combustion corresponds to the condition where the oxygen uncoupling reaction rate is maximized. This condition is reached when the oxygen concentration in

Eq. (20) is considered to be zero, corresponding to the asymptotic limit in which all the O_2 released is consumed by the fuel and there is not an excess of O_2 in gases [25].

On the other hand, the solids inventory in the air reactor was calculated considering an air excess of 20%. The average oxygen concentration in the air reactor was those that fulfil Eq. (33), in this case 11 vol.%; see reference [26] for more information.

$$\frac{\Delta X_g}{\left[\overline{\frac{dX_i}{dt}}\right]_{O_2}} = \int_{X_{g,in}}^{X_{g,out}} \frac{dX_g}{\left[\overline{\frac{dX_i}{dt}}\right]} \tag{33}$$

The residence time distribution of particles in the reactor was also considered to calculate the average reaction rate. Assuming perfect mixing of solids in the reactors, the average reaction rate was calculated as [26]:

$$\left(\overline{\frac{dX_i}{dt}}\right) = \int_0^{t_c} \left[\frac{dX_i}{dt}\right] \frac{e^{-t/t_m}}{t_m} dt \tag{34}$$

This equation considers particles enter to the reactor partially converted. The reaction time necessary to reach complete conversion will be t_c, being this value the upper limit of the integration of Eq. (34). Following the method presented in [26], t_c is defined here for the nucleation model as:

$$t_c = \frac{1}{k}\left(-\ln \overline{X}_{Red,inFR}\right)^{3/4} \tag{35}$$

Thus, initial reaction rate was calculated for conversion $X_{red} = 0$, and t_c corresponded to the time reaching complete reduction, in this case for $X_{red} = 1 - \overline{X}_{Red,inFR}$.

The expression that describe the reactivity using a nucleation model is the following

$$\left[\frac{dX_{Red}}{dt}\right] = \frac{4}{3} k \cdot t^{1/3} \cdot e^{-(k \cdot t)^{4/3}} \tag{36}$$

Parameter k includes the kinetic constant and the function of the oxygen concentration.

$$k = k'_{\mathrm{Red}} \left(1 - cC_{O_2}^{1/n}\right)\left(1 - \frac{C_{O_2}}{C_{eq}}\right) \tag{37}$$

t_m is the mean residence time of the oxygen carrier particles in the fuel reactor, which is dependent on the solid recirculation rate and on the reactor size.

$$t_m = \frac{m_{OC,FR}}{\dot{m}_{OC}} = \frac{\Delta X_{\mathrm{Red}}}{\left[\overline{\frac{dX_{\mathrm{Red}}}{dt}}\right]} \tag{38}$$

The average reactivity has been expressed to consider that the oxygen carrier can be introduced to the fuel reactor with a mean solid conversion reduction, $\overline{X}_{\mathrm{Red},inFR}$, higher than 0. Following nucleation model, it was assumed that the unconverted solid was in the surface of the particle. It is worth noting that the minimum oxygen inventory calculated in this section is a function of the oxygen carrier reactivity, and corresponds to the amount of solids to supply oxygen at the required rate determined by the coal feeding rate. Later on, the oxygen consumption by the coal will be further analysed, which will depend on the coal reactivity.

The minimum oxygen carrier inventory in the fuel or air reactor was calculated considering complete conversion in each reactor. Fig. 11 shows the minimum oxygen carrier inventories for both fuel and air reactor as a function of the variation in the oxygen carrier conversion at 1223 K. It can be seen that low values of variation of oxygen carrier conversion gives high values of oxygen carrier circulation rate and low amount of solid inventories in both reactors. If a value of $\Delta X_{OC} = 0.1$ was assumed, the minimum values of oxygen carrier inventories are 160 kg/MW_{th} and 95 kg/MW_{th} for the fuel and air reactor, respectively. A high solid inventory in the fuel reactor (235 kg/MW_{th}) was experimentally used in combustion tests in a 1.5 kW_{th} CLOU unit with this oxygen carrier [8]. However, there was an O_2 excess at the fuel reactor exit,

therefore lower inventories would be possible in that unit with complete combustion of the fuel.

4.2. Carbon capture efficiency for different fuels

In addition to the solids inventory needed to transfer the required oxygen to full combustion determined by the coal feeding rate, it is necessary to reach high combustion efficiency in the fuel reactor. So, the solids residence time in the fuel reactor must allow the char conversion, which is related to the CO_2 capture efficiency. It is worth noting that unconverted char in the fuel reactor reaches the air reactor, where it will be burnt to CO_2 which is not captured. Thus, the CO_2 capture efficiency would depend on the solid inventory in the fuel reactor.

The performance of the fuel reactor in a CLOU system is influenced by the pseudo-equilibrium reached between the oxygen released by the oxygen carrier and the oxygen consumed by fuel. Therefore, the oxygen balance in the fuel reactor must consider the oxygen release from the oxygen carrier and the different uses of this oxygen, for conversion of char, volatiles and O_2 concentration in gas stream:

$$\left(-r_{O_2}\right)_{OC} = \left(r_{O_2}\right)_{C} + \left(r_{O_2}\right)_{vol} + \left(r_{O_2}\right)_{gas} \tag{39}$$

The oxygen release rate depends on the oxygen carrier reactivity and the oxygen concentration in the reactor

$$\left(-r_{O_2}\right)_{OC} = R_{OC} m_{OC,FR} \left[\frac{\overline{dX_{\mathrm{Red}}}}{dt}\right] \tag{40}$$

The oxygen released from the oxygen carrier is used to:

1. To burn carbon in char particles. During TGA tests of char combustion with gaseous O_2, constant reaction rate with time was observed [10, 32]. Thus, the char reaction rate can be calculated by

$$\left(r_{O_2}\right)_C = \frac{M_{O_2}}{M_C}\frac{m_{C,FR}}{1-X_C}\left[\overline{\frac{dX_C}{dt}}\right] \tag{41}$$

2. To burn volatile matter. It is assumed complete combustion of volatile matter. The oxygen reacted with volatile matter is the difference between the oxygen demand of the solid fuel fed and the oxygen demand of the fixed carbon.

$$\left(r_{O_2}\right)_{vol} = \dot{m}_{coal}\left\{m_O - \frac{M_{O_2}}{M_C}\left[C_{fix}\right]\right\} \tag{42}$$

3. To accumulate in the exit gas stream. Oxygen can be present in the gaseous stream from the fuel reactor, but always at concentrations below the equilibrium concentration at the reactor temperature. The rate of oxygen release in the gaseous stream depends on the gas at the fuel reactor exit, which in turn depends on the gas inlet to the fuel reactor inlet.

$$\left(r_{O_2}\right)_{gas} = M_{O_2}\left[F_{gas}y_{O_2}\right]_{outFR} \tag{43}$$

$\left(r_{O_2}\right)_{gas}$ only depends on oxygen concentration and $\left(r_{O_2}\right)_C$ also depends on char concentration in the fuel reactor. To determine the char concentration, a carbon balance was done considering the different streams where carbon is: carbon in fuel, carbon in volatiles, carbon in converted char in the fuel reactor, and carbon in the solids stream from the fuel reactor.

$$F_{C,SF} = F_{C,vol} + X_C F_{C,char} + \left(1-X_C\right)F_{C,char} \tag{44}$$

Each carbon flow is calculated as:

$$F_{C,coal} = \frac{1}{M_C} \dot{m}_{coal} \left[C_{coal} \right] \tag{45}$$

$$F_{C,vol} = \frac{1}{M_C} \dot{m}_{coal} \left[C_{coal} - C_{fix} \right] \tag{46}$$

$$F_{C,char} = \frac{1}{M_C} \dot{m}_{coal} \left[C_{fix} \right] \tag{47}$$

$$\left(1 - X_C\right) F_{C,char} = \frac{1}{M_C} \dot{m}_{OC} \frac{f_{C,FR}}{1 - f_{C,FR}} \left(1 - \eta_{CSS}\right) \tag{48}$$

f_C being the mass fraction of carbon in solids in the fuel reactor:

$$f_C = \frac{m_{C,FR}}{m_{OC,FR} - m_{C,FR}} \tag{49}$$

The char fraction f_C affects to the solids transfer to the air reactor and the oxygen consumed in the fuel reactor. The effect of a carbon stripper efficiency, η_{CSS}, on char conversion is also considered in Eq. (48). A carbon stripper makes a selective recirculation of uncorveted char particles to the fuel reactor from the solids stream exiting the fuel reactor in order to minimize the flow of unconverted carbon in the air reactor [32], thus obtaining high CO_2 capture efficiencies [10, 32].

By fixing the mass of oxygen carrier in the fuel reactor, an iterative process can be done modifying the oxygen concentration and the mass fraction of carbon in the fuel reactor to obtain the oxygen generation rate and the consumption rate in Eqs. (40) and (41). The objective of the iterative process was to fulfil simultaneously the oxygen and carbon balances showed in Eqs. (39) and (44). Once each carbon flow is known, the CO_2 capture efficiency, η_{CC}, can be obtained for the assumed solids inventory.

$$\eta_{CC} = \frac{F_{C,vol} + X_C F_{C,char}}{F_{C,coal}} \tag{50}$$

It is worth noting that the CO_2 capture efficiency also depends on the solids circulation flow rate because: (1) the circulation of solids affects to the solids residence time, and therefore to the reactivity of oxygen carrier; and (2) affects to the carbon flow exiting the fuel reactor.

In this work, three fuels have been considered for the analysis: a high reactive bituminous coal (HRB), a low volatile bituminous coal (LVB) and a lignite. These coals were tested before at the continuous CLOU 1.5 kW_{th} unit [8, 10], showing different behaviour during the combustion tests. The char reactivity kinetic parameters needed for this study have been taking from Hurt and Mitchell [33]. Proximate and ultimate analysis and the corresponding kinetic parameters are shown in Table 6 for each coal.

Fig. 12(a) shows the O_2 concentration at the fuel reactor outlet as a function of the oxygen carrier conversion using the lignite fuel and different fuel reactor solid inventories (150, 250, 500 and 1500 kg/MW_{th}). Fuel reactor temperature was 1223 K and the use of a carbon separation system ($\eta_{CSS} = 0$) was not considered. The O_2 concentration at equilibrium conditions is also included for comparison purposes. It can be observed that the oxygen concentration decreases when the variation of the conversion increases. This is due to the fact that more coal is converted in the fuel reactor and the average oxygen carrier reactivity decreases as ΔX_{OC} increases, see Eq. (39). It can be also seen that the oxygen concentration increases when the solids inventory in the fuel reactor increases, because there is more oxygen in solids available for oxygen uncoupling. Underline that when the CO_2 capture efficiency is low there are O_2 at the fuel reactor outlet. This means, that this oxygen carrier is highly reactive and can release O_2 although the residence time in the fuel reactor is not enough to convert completely the char.

Fig. 12(b) shows the CO_2 capture efficiency as a function of the variation of the oxygen carrier conversion for same conditions. CO_2 capture efficiency increases when the solid inventory and the oxygen carrier conversion increase due to the associated increase in the solids residence time. Note that all lines converge to a CO_2 capture value of 24% at $\Delta X_{OC} = 0$ which corresponds to the combustion of the volatile matter of this coal. At high values of the solids conversion, the increase in the CO_2 capture efficiency is smoother. This behaviour is due to two additive reasons: 1) the residence time in the fuel reactor is inversely proportional to the conversion variation, producing that the char conversion is not proportional to the variation of oxygen carrier conversion; 2) a less O_2 concentration in the fuel reactor decrease the char conversion rate in the fuel reactor. In fact, the CO_2 capture efficiency can decrease slightly at high values of ΔX_{OC}. Therefore, a maximum in the CO_2 capture efficiency for each solids inventory in the fuel reactor was observed by changing the solids conversion variation. This maximum is due to the oxygen concentration decrease toward 0, and the effect of low oxygen concentration on the decrease of the char combustion rate is higher than the beneficial effect of the residence time increase.

CO_2 capture efficiencies higher than 90% can be only reached with oxygen carrier inventories higher than 500 kg/MW_{th} and $\Delta X_{OC} > 0.5$, without the use of a carbon separation system ($\eta_{CSS} = 0$). Therefore, it is recommended to work with high values of ΔX_{OC}, i.e. low solids circulation rate to obtain high CO_2 capture efficiencies.

Fig. 13(a) shows the O_2 concentration at the outlet of the fuel reactor as a function of the fuel reactor solids inventory for the three different coals (HRB, lignite and LVB). Fuel reactor temperature was 1223 K and the use of a carbon separation system ($\eta_{CSS} = 0$) was not considered. It can be observed that the O_2 concentration increases with the inventory in the fuel reactor due to the increase of solids generating oxygen. The O_2

concentration is very similar for the lignite and LVB, but it is lower for the HRB, due to the high amount of volatiles that the HRB contains, which consume more O_2. As an example, for fuel reactor solids inventories <600 kg/MW_{th}, oxygen concentrations at fuel reactor outlet are of the order of 1 vol.% which are lower than that found in oxy-combustion process for coal.

The effect of fuel reactor solids inventory on the CO_2 capture efficiency was also evaluated for the different coals: HRB, lignite and LVB. Fig. 13(b) shows the variation of the CO_2 capture efficiency as a function of the solid inventory in the fuel reactor for these coals at the same conditions, but considering a solid conversion variation of ΔX_{OC} =0.7. In all cases the CO_2 capture efficiency increases with the solids inventory because of a higher solid residence time and higher oxygen availability. It can be seen that for the high reactive coals, i.e. HRB and lignite, it is possible to reach high CO_2 capture efficiencies (≥95%) with around 600 kg/MW_{th} in the fuel reactor. However, for low reactive coals, i.e. LVB, it is necessary higher values of solids inventory to achieve high CO_2 capture efficiency, with values near 1500 kg/MW_{th}. Moreover, Fig 13(b) shows experimental results obtained in the 1.5 kW_{th} continuous unit for CLOU process with different coals: HVB, lignite and LVB [8,10]. It can be seen that experimental results match with data obtained from the model for each coal simulated. Fig. 13(b) also shows the CO_2 capture efficiency for a LVB when a carbon stripper with a 90% of efficiency was included in the simulation. It can be seen the important effect of this separation unit allowing high CO_2 capture efficiencies even with low values of solids inventories, 99% with 700 kg/MW_{th}. Therefore, for low reactive coals it is necessary to use a carbon stripper to reach high CO_2 capture rates. But even for reactive coals, the use of an efficient carbon tripper reduces also the oxygen carrier inventories in the fuel reactor and the SO_2 emissions in the air reactor [11, 34].

It is worth noting that the fuel reactor solids inventory needed to supply the stoichiometric oxygen flow rate to burn a lignite (about 300 kg/MW_{th}, with $\Delta X_{OC} = 0.7$; see Fig. 11) is lower than the solids inventory needed to reach a CO_2 capture higher than 95% without a carbon stripper (≈600 kg/MW_{th}). This fact agree with previous results obtained from the analysis of the oxygen carrier reactivity [25] and results obtained in a CLOU unit [8, 10]. It can be concluded that the kinetic parameters determined together with the simulation tool developed in this work, configure a useful instrument for the design and optimization of CLOU process.

5. Conclusions

Reaction rates of reduction and oxidation of a Cu-based oxygen carrier (60 wt.% of CuO and 40 wt.% of $MgAl_2O_4$) for CLOU process has been measured by TGA to determine the redox kinetic. Relevant reactions were decomposition of CuO to Cu_2O and oxidation of Cu_2O to CuO. A nucleation model for the variation of the solid conversion with time and a Langmuir-Hinshelwood surface kinetic control together with Freundlich's isotherm was valid to predict the experimental data in a broad range of O_2 concentration and temperatures. In fact good predictions were obtained even at O_2 concentrations very close to the equilibrium conditions.

The kinetic model was further used to analyze the design and operation conditions of CLOU process using this oxygen carrier. Minimum solids inventory of 160 kg/MW_{th} in the fuel reactor and 95 kg/MW_{th} in air reactor were determined to transfer the oxygen flow demanded for full combustion of the coal. The CO_2 capture efficiency as a function of the oxygen carrier circulation rate and the fuel reactor solids inventory for three different coals have been also estimated. For high reactive coals, i.e. HRB and

lignite, it would be possible to reach high CO_2 capture rates (≥95%) with 600 kg/MW_{th}. However, for low reactive coals, i.e. LVB, 1500 kg/MW_{th} would be needed to achieve high CO_2 capture efficiencies. These results highlight the need of using an efficient carbon stripper which allows CO_2 capture efficiencies higher than 95% with low solids inventories.

ACKNOWLEDGEMENT

This work was supported by the European Commission, under the RFCS program (ACCLAIM Project, Contract RFCP-CT-2012-00006), the Spanish Ministry of Science and Innovation (MICINN Project: ENE2011-26354) and the European Union FEDER Funds. I. Adánez-Rubio thanks CSIC for the JAE fellowship co-financed by the European Social Fund.

NOTATION

Symbols

a	Active sites in the particles surface (-)
C_i	Carbon concentration in the fuel reactor ($mol \cdot s^{-1}$)
C_{coal}	Carbon concentration in the coal ($kg \cdot kg^{-1}$)
C_{fix}	Carbon concentration in the fixed carbon ($kg \cdot kg^{-1}$)
C_{O_2}	Oxygen concentration ($mol \cdot m^{-3}$)
$C_{O_2,eq}$	Oxygen concentration at equilibrium conditions ($mol \cdot m^{-3}$)
$C_{O_2,Ox}$	Oxygen concentration during oxidation reaction ($mol \cdot m^{-3}$)
$C_{O_2,Red}$	Oxygen concentration during reduction reaction ($mol \cdot m^{-3}$)
c	Adsorption rate constant ($(m^3 \cdot mol^{-1})^{1/n}$)
c_0	Preexponenial factor of adsorption rate constant ($(m^3 \cdot mol^{-1})^{1/n}$)
E_1	Global activation energy ($J \cdot mol^{-1}$), Eq. (6)
E_2	Kinetic activation energy ($J \cdot mol^{-1}$), Eq. (7)
E_C	Activation energy of parameter c ($J \cdot mol^{-1}$)
E_0	Activation energy of char combustion reaction ($J \cdot mol^{-1}$)
E_{Ox}	Activation energy of oxidation reaction ($J \cdot mol^{-1}$)
E_{Red}	Activation energy of reduction reaction ($J \cdot mol^{-1}$)
E_{th}	Thermodinamic activation energy ($J\ mol^{-1}$), Eq. (5)
F_i	Molar flow of compound i ($mol \cdot s^{-1}$)
f_C	Mass fraction of carbon in solid in the fuel reactor (-)
$f_{C,fix}$	Mass fraction of fix carbon in coal (-)
$f_{C,vol}$	Mass fraction of carbon in volatiles (-)
K_1	Equilibrium constant of the chemical decomposition and adsorbed O_2 (-)
K_2	Equilibrium constant of the desorption of adsorbed O_2 (-)
K_3	Equilibrium constant of the adsorption of O_2 over the surface of Cu_2O (-)
K_4	Equilibrium constant of the oxidation of Cu_2O to CuO (-)
k	Kinetic parameter for simulation process (s^{-1}), Eq. (37)
k_1	Kinetic constant (s^{-1}), Eq. (6)
k_2	Kinetic constant ($m^{-3} \cdot mol^{-1} \cdot s^{-1}$), Eq. (7)
k_f	Chemical reaction rate constant for the forward process in CuO-Cu_2O equilibrium ($mol \cdot m^{-2} \cdot s^{-1}$)
k_b	Chemical reaction rate constant for the backward process in CuO-Cu_2O equilibrium (s^{-1})
k_A	Constant desorption rate of adsorbed O_2 (s^{-1})
k_D	Constant adsorption rate of O_2 over the surface of Cu_2O (s^{-1})
k_{Red}	Chemical reaction rate constant for the reduction of CuO to Cu_2O ($kg \cdot m^{-2} \cdot s^{-1}$)
k_0	Preexponenial factor of chemical reaction rate constant for the char combustion ($m^3 \cdot mol^{-1} \cdot s^{-1}$)
k_{Ox}	Chemical reaction rate constant for the oxidation of Cu_2O to CuO ($kg \cdot m^{-2} \cdot s^{-1}$)
k'_{Red}	Effective chemical reaction rate constant for the reduction of CuO to Cu_2O (s^{-1})
k'_{Ox}	Effective chemical reaction rate constant for the oxidation of Cu_2O to CuO ($(m^3 \cdot mol^{-1})^{1/n} \cdot s^{-1}$)
$k'_{Red,0}$	Preexponenial factor of chemical reaction rate constant for the reduction of CuO to Cu_2O (s^{-1})

$k'_{Ox,0}$	Preexponenial factor of chemical reaction rate constant for the oxidation of Cu_2O to CuO ($(m^3 \cdot mol^{-1})^{1/n} \cdot s^{-1}$)
M_i	Atomic or molecular weigh of i elements or compound ($kg \cdot mol^{-1}$)
m	Mass of the sample at each time in TGA (kg)
$\dot{m}_{coal}$	Mass-based flow of coal fed-in to the fuel reactor ($kg \cdot s^{-1}$)
$m_{C,FR}$	Carbon inventory in the fuel reactor ($kg \cdot MW_{th}^{-1}$)
m_O	Stoichiometric mass of O_2 to convert 1 kg of coal ($kg \cdot kg^{-1}$)
$\dot{m}_{OC}$	Solids circulation rate ($kg \cdot s^{-1} \cdot MW_{th}^{-1}$)
$m_{OC,i}$	Oxygen carrier inventory in the reactor i ($kg \cdot MW_{th}^{-1}$)
m_{ox}	Mass of the oxygen carrier sample fully oxidized (kg)
m_{red}	Mass of the oxygen carrier sample fully reduced (kg)
$m_{s,FR}$	Mass of solids in the fuel reactor (kg)
N	Nucleation reaction order (-)
n	Langmuir-Hinshelwood reaction order (-)
n'	Reaction order (-)
p	Reaction order for char combustion (-)
R_g	Gas constant (8.314 $J \cdot mol^{-1} \cdot K^{-1}$)
R_{OC}	Oxygen transport capability (-)
$(-r_{O_2})_C$	Conversion rate of the char (s^{-1})
$(-r_{O_2})_{gas}$	Oxygen release in gas stream (s^{-1})
$(-r_{O_2})_{OC}$	Oxygen release rate of the oxygen carrier (s^{-1})
$(-r_{O_2})_{vol}$	Conversion rate of the volatiles (s^{-1})
$(r_{Ox})_{OC}$	Oxygen carrier oxidation rate (s^{-1})
$(-r_{Red})_{OC}$	Oxygen carrier reduction rate (s^{-1})
S_{CuO}	Specific surface area of CuO ($m^2 \cdot kg^{-1}$)
T	Temperature (K)
t_c	Reaction time necessary to reach oxygen carrier complete conversion (s)
t_m	Mean residence time of the oxygen carrier particles in the fuel reactor (s)
X	Solid conversion (-)
X_c	Char conversion (-)
X_g	Gas conversion at the air reactor (-)
$X_{g,in}$	Gas conversion at the air reactor inlet flow (-)
$X_{g,out}$	Gas conversion at the air reactor outlet flow (-)
$\overline{X}_{Red,inFR}$	Inlet mean oxygen carrier reduction conversion to the fuel reactor (-)
X_{Red}	Oxygen carrier reduction conversion (-)
X_{Ox}	Oxygen carrier oxidation conversion (-)
y_{O_2}	Molar fraction of oxygen (-)
ΔX_g	Variation of the gases conversion
ΔX_{OC}	Variation of the oxygen carrier conversion

Greek letters

η_{CC}	Carbon capture efficiency (-)
η_{CSS}	Efficiency of the carbon stripper (-)

ϕ	Characteristic reactivity (-)
θ	Fraction of active sites occupied by O_2 (-)

Acronyms

BET	Brunauer-Emmett-Teller
BFBR	Batch Fluidized Bed Reactor
CLAS	Chemical Looping Air Separation
CLC	Chemical Looping Combustion
CLOU	Chemical Looping with Oxygen Uncoupling
FBR	Fix Bed Reactor
HRB	High Reactive Bituminous coal
LHV	Low Heating Value ($kJ \cdot kg^{-1}$)
LVB	Low Volatile Bituminous coal
TGA	Thermogravimetric analyser
XRD	X-ray diffractometer

Subscripts

AR	Air reactor
C,char	Carbon in the coal char
C,coal	Carbon in the coal
C,vol	Carbon in the volatiles
FR	Fuel reactor
OC	Oxygen carrier
Ox	Oxidation reaction
Red	Reduction reaction

REFERENCES

[1] T. Mattisson, A. Lyngfelt, H. Leion, Chemical-looping with oxygen uncoupling for combustion of solid fuels, International Journal of Greenhouse Gas Control, 3 (2009) 11-19.

[2] P. Gayán, I. Adánez-Rubio, A. Abad, L. de Diego, F. García Labiano, J. Adánez, Development of Cu-based oxygen carriers for Chemical-Looping with Oxygen Uncoupling (CLOU) process, Fuel, 96 (2012) 226-238.

[3] I. Adánez-Rubio, P. Gayán, F. García-Labiano, L. de Diego, J. Adánez, A. Abad, Development of CuO-based oxygen-carrier materials suitable for Chemical-Looping with Oxygen Uncoupling (CLOU) process, Energy Procedia, 4 (2011) 417-424.

[4] I. Adánez-Rubio, M. Arjmand, H. Leion, P. Gayán, A. Abad, T. Mattisson, A. Lyngfelt, Investigation of Combined Supports for Cu-Based Oxygen Carriers for Chemical-Looping with Oxygen Uncoupling (CLOU), Energy Fuels, 27 (2013) 3918-3927.

[5] M. Rydén, H. Leion, T. Mattisson, A. Lyngfelt, Combined oxides as oxygen-carrier material for chemical-looping with oxygen uncoupling, Appl. Energy, 113 (2014) 1924-1932.

[6] J. Adanez, A. Abad, F. Garcia Labiano, P. Gayan, L. de Diego, Progress in Chemical-Looping Combustion and Reforming technologies, Progr. Energy Combust. Sci., 38 (2012) 215-282.

[7] T. Mattisson, Materials for Chemical-Looping with Oxygen Uncoupling, ISRN Chemical Engineering, 2013 (2013) 19.

[8] A. Abad, I. Adánez-Rubio, P. Gayán, F. García Labiano, L. de Diego, J. Adánez, Demonstration of chemical-looping with oxygen uncoupling (CLOU) process in a 1.5kW_{th} continuously operating unit using a Cu-based oxygen-carrier, International journal of greenhouse gas control, 6 (2012) 189-200.

[9] I. Adánez-Rubio, P. Gayán, A. Abad, L. de Diego, F. García Labiano, J. Adánez, Evaluation of a Spray-Dried CuO/$MgAl_2O_4$ Oxygen Carrier for the Chemical Looping with Oxygen Uncoupling Process, Energy Fuels, 26 (2012) 3069-3081.

[10] I. Adánez-Rubio, A. Abad, P. Gayán, L.F. de Diego, F. García Labiano, J. Adánez, Performance of CLOU process in the combustion of different types of coal with CO_2 capture, International journal of greenhouse gas control, 12 (2013) 430-440.

[11] I. Adánez-Rubio, A. Abad, P. Gayán, F. García Labiano, L. de Diego, J. Adánez, The fate of sulphur in the Cu-based Chemical Looping with Oxygen Uncoupling (CLOU) Process, Appl. Energy, 113 (2014) 1855-1862.

[12] I. Adánez-Rubio, A. Abad, P. Gayán, L.F. de Diego, F. García-Labiano, J. Adánez, Biomass combustion with CO_2 capture by chemical looping with oxygen uncoupling (CLOU), Fuel Process. Technol., 124 (2014) 104-114.

[13] F. Garcia-Labiano, L.F. de Diego, J. Adánez, A. Abad, P. Gayan, Reduction and oxidation kinetics of a copper-based oxygen carrier prepared by impregnation for chemical-looping combustion, Ind. Eng. Chem. Res., 43 (2004) 8168-8177.

[14] A. Sahir, H. Sohn, H. Leion, J. Lighty, Rate Analysis of Chemical-Looping with Oxygen Uncoupling (CLOU) for Solid Fuels, Energy Fuels, 26 (2012) 4395-4404.

[15] C. Clayton, K. Whitty, Measurement and modeling of decomposition kinetics for copper oxide-based chemical looping with oxygen uncoupling, Appl. Energy, (2013).

[16] D. Chadda, J.D. Ford, M.A. Fahim, Chemical energy storage by the reaction cycle CuO/Cu_2O, International Journal of Energy Research, 13 (1989) 63-73.

[17] E.M. Eyring, G. Konya, J.S. Lighty, A.H. Sahir, A.F. Sarofim, K. Whitty, Chemical Looping with Copper Oxide as Carrier and Coal as Fuel, Oil Gas Sci. Technol., 66 (2011) 209-221.

[18] H. Song, K. Song, E. Shah, T. Doroodchi, B. Wall, Moghtaderi, Analysis on Chemical Reaction Kinetics of CuO/SiO_2 Oxygen Carriers for Chemical Looping Air Separation, Energy Fuels, 28 (2014) 173-182.

[19] K. Whitty, C. Clayton, Measurement and Modeling of Kinetics for Copper-Based Chemical Looping with Oxygen Uncoupling, 2nd International Conference on Chemical Looping 26-28 September 2012, Darmstadt. Germany, (2012).

[20] S. Peterson, G. Konya, C. Clayton, R. Lewis, B. Wilde, E. Eyring, K. Whitty, Characteristics and CLOU Performance of a Novel SiO2-Supported Oxygen Carrier Prepared from CuO and β-SiC, Energy Fuels, 27 (2013) 6040-6047.

[21] K. Wang, Q. Yu, Q. Qin, Reduction Kinetics of Cu-Based Oxygen Carriers for Chemical Looping Air Separation, Energy Fuels, 27 (2013) 5466-5474.

[22] M. Arjmand, M. Keller, H. Leion, T. Mattisson, A. Lyngfelt, Oxygen Release and Oxidation Rates of $MgAl_2O_4$-Supported CuO Oxygen Carrier for Chemical-Looping Combustion with Oxygen Uncoupling (CLOU), Energy Fuels, 26 (2012) 6528-6539.

[23] Y. Zhu, K. Mimura, J.W. Lim, M. Isshiki, Q. Jiang, Brief review of oxidation kinetics of copper at 350 °C to 1050 °C, Metall. Mater. Trans. A, 37 (2006) 1231-1237.

[24] S.Y. Chuang, J.S. Dennis, A.N. Hayhurst, S.A. Scott, Kinetics of the Oxidation of a Co-precipitated Mixture of Cu and Al2O3by O2for Chemical-Looping Combustion, Energy Fuels, 24 (2010) 3917-3927.

[25] I. Adánez-Rubio, A. Abad, P. Gayán, L. de Diego, F. García Labiano, J. Adánez, Identification of operational regions in the Chemical-Looping with Oxygen Uncoupling (CLOU) process with a Cu-based oxygen carrier, Fuel, 102 (2012) 634-645.

[26] A. Abad, J. Adánez, F. García Labiano, L. de Diego, P. Gayán, J. Celaya, Mapping of the range of operational conditions for Cu-, Fe-, and Ni-based oxygen carriers in chemical-looping combustion, Chem. Eng. Sci., 62 (2007) 533-549.

[27] F. García Labiano, L. de Diego, J. Adánez, A. Abad, P. Gayán, Temperature variations in the oxygen carrier particles during their reduction and oxidation in a chemical-looping combustion system, Chem. Eng. Sci., 60 (2005) 851-862.

[28] C.N. Hinshelwood, The Kinetics of Heterogeneous Reactions, in: Kinetics of Chemical Change Clarendon Press, Oxford, 1940, pp. 178-234.

[29] F. García-Labiano, A. Abad, L.F. de Diego, P. Gayán, J. Adánez, Calcination of calcium-based sorbents at pressure in a broad range of CO_2 concentrations, Chem. Eng. Sci., 57 (2002) 2381-2393.

[30] B.V. Erofe'Ev, Comptes Rendus de l'Académie des Sciences de l'Urss, (1946) 511.

[31] A. Abad, J. Adánez, A. Cuadrat, F. García Labiano, P. Gayán, L. de Diego, Kinetics of redox reactions of ilmenite for chemical-looping combustion, Chem. Eng. Sci., 66 (2011) 689-702.

[32] Y. Cao, W.P. Pan, Investigation of chemical looping combustion by solid fuels. 1. Process analysis, Energy and Fuels, 20 (2006) 1836-1844.

[33] R. Hurt, R. Mitchell, Unified high-temperature char combustion kinetics for a suite of coals of various rank, Symposium, International, on Combustion, 24 (1992) 1243-1250.

[34] J. Adánez, P. Gayán, I. Adánez-Rubio, A. Cuadrat, T. Mendiara, A. Abad, F. García-Labiano, L.F. de Diego, Use of Chemical-Looping processes for coal combustion with CO_2 capture, Energy Procedia, 37 (2013) 540-549.

Caption of tables

Table 1. Relevant kinetic studies for CLOU conditions on CuO reduction and Cu_2O oxidation.

Table 2. Properties of the oxygen carrier Cu60MgAl.

Table 3. Experimental conditions for TGA tests. O_2 concentrations at thermodinamic equilibrium also shown.

Table 4. Correlation coefficients of the linear dependence of $(-\ln(1-X_{red}))^N$ vs time plots for various values of N for Cu60MgAl oxygen carrier. T_{Red} = 1273 K; $y_{O_2,Red}$ = 4 vol.%; T_{Ox} = 1173 K; $y_{O_2,Ox}$ = 6 vol.%;

Table 5. Kinetic parameters determined in this work for Cu60MgAl.

Table 6. Properties and kinetic parameters for the different coals considered taken from [33].

Table 1. Relevant kinetic studies for CLOU conditions on CuO reduction and Cu_2O oxidation.

Oxygen carrier (wt.% CuO)	Support	Preparation method[a]	dp(μm)	Facility[b]	*T* (K)	E_A(kJ/mol) Global	E_A(kJ/mol) Kinetic	Model	Ref.
Reduction									
Pure	----	----	10	TGA	1033-1183	313	----	First order	[14]
Pure	----	----	104-152	TGA	1123-1233	327	----	First order	[17]
40	$MgAl_2O_4$	FG	125-180	bFBR	1123-1173	139	----	Avrami-Erofeev (N=2)	[22]
42	SiC	I	105-150	TGA	1123-1223	220	----	First order	[20]
60	SiO_2	MM	200-315	TGA	1073-1223	145	----	Avrami-Erofeev (N=3)	[21]
20	SiO_2	IW	< 45 75-125 125-210	TGA bFBR FxBR	1173-1273	170	----	First order	[19]
18	SiO_2	I	106-150	TGA	1073-1173 1173-1248	315 176	----	Avrami-Erofeev (N=2)	[18]
60	TiO_2	MM	200-315	TGA	1073-1223	155	----	Avrami-Erofeev (N=3)	[21]
50	TiO_2	MM	< 45 75-125 125-210	TGA bFBR FxBR	1173-1273	180	----	First order	[19]
50	TiO_2	MM	< 45	TGA	1073-1173	284	58	First order	[15]
60	ZrO_2	MM	200-315	TGA	1073-1223	153	----	Avrami-Erofeev (N=3)	[21]
55	ZrO_2	FG	< 45 75-125 125-210	TGA bFBR FxBR	1073-1273	147	----	First order	[19]
45	ZrO_2	FG	< 45	TGA	1048-1198	264	67	First order	[15]
40	ZrO_2	FG	125-180	bFBR	1173-1258	281	20	First order	[14]
Oxidation									
Pure	----	----	disc (5 mm i.d[c])	TGA	> 1173	173-98	----	First order	[23]
Pure	----	----	10	TGA	673-773	76.5	----	First order	[14]
18	SiO_2	I	106-150	TGA	1073-1173 1173-1248	3 -43	----	Phase boundary reaction (N=2)	[18]
55	ZrO_2	FG	< 45 75-125 125-210	TGA bFBR FxBR	1123-1273	----	202	First order	[19]

[a]Key for preparation method:
I = Impregnation
IW = Incipient wetness
MM = Mechanical mixing
FG = Freeze granulation

[b]Key for facility:
bFBR = batch fluidized bed reactor
FxBR = Fixed bed reactor
TGA = thermogravimetric analyzer

[c]i.d = inner diameter

Table 2. Properties of the oxygen carrier Cu60MgAl.

CuO content (wt.%)	60
Oxygen transport capacity, R_{OC} (wt.%)*	6
Crushing strength (N)	2.4
Skeletal density (kg/m^3)	4600
Porosity (%)	16.1
Specific surface area, BET (m^2/g)	< 0.5
XRD main phases	CuO, $MgAl_2O_4$

*Reduction from CuO to Cu_2O

Table 3. Experimental conditions for TGA tests. O_2 concentrations at thermodinamic equilibrium also shown.

Reduction			**Oxidation**		
T (K)	y_{O_2} (%) *	$y_{O_2,eq}$ (%)	T (K)	y_{O_2} (%) *	$y_{O_2,eq}$ (%)
			1123	21	0.4
1148	0	0.8	1148	21	0.8
1173	0	1.4	1173	21, 11, 9, 4, 2.5	1.4
1198	0	2.4	1198	21	2.4
1223	0, 1.5, 2.5	4.2	1223	21	4.2
1248	0, 1.5, 4	7.0	1248	21	7.0
1273	0, 1.5, 4, 6, 8, 9	11.6	1273	21	11.6

*N_2 to balance

Table 4. Correlation coefficients of the linear dependence of $(-\ln(1-X_{red}))^N$ vs time plots for various values of N for Cu60MgAl oxygen carrier. T_{Red} = 1273 K; $y_{O_2,Red}$ = 4 vol.%; T_{Ox} = 1173 K; $y_{O_2,Ox}$ = 6 vol.%;

N	Reduction	Oxidation
3/2	0.9017	0.9570
1	0.9769	0.9970
3/4	0.9961	0.9977
2/3	0.9951	0.9926
1/2	0.9838	0.9703

Table 5. Kinetic parameters determined in this work for Cu60MgAl.

Reduction	
$k'_{Red,0}$ (s^{-1})	$3.6 \cdot 10^{9}$
E_{Red} (kJ mol^{-1})	$2.7 \cdot 10^{2}$
c_0 ((m^3 mol^{-1})$^{1/n}$)	$1.8 \cdot 10^{-10}$
E_C (kJ mol^{-1})	$-2.4 \cdot 10^{2}$
n	0.5
Oxidation	
$k'_{Ox,0}$ (($m^3 \cdot mol^{-1}$)$^{1/n} \cdot s^{-1}$)	$6.2 \cdot 10^{-1}$
E_{Ox} (kJ mol^{-1})	$3.2 \cdot 10^{1}$
n	1.2

Table 6. Properties and kinetic parameters for the different coals considered taken from [33].

	Lignite	Low Volatile Bituminous	High Volatile Bituminous
Proximate Analysis (wt.%)			
Moisture	12.6	2.0	2.3
Volatile matter	28.6	17.1	33.0
Fixed carbon	33.6	68.8	55.9
Ash	25.2	12.1	8.8
Ultimate Analysis (wt.%)			
C	45.4	75.8	65.8
H	2.5	3.7	3.3
N	0.6	1.9	1.6
S	5.2	0.4	0.6
O[(1)]	8.5	4.1	17.6
Kinetic parameters			
k_0 ($m^3 \cdot mol^{-1} \cdot s^{-1}$)	$2.7 \cdot 10^7$	$1.8 \cdot 10^7$	$1.5 \cdot 10^5$
E_0 (kJ mol^{-1})	91.5	94.1	64.0
p	0.5	0.5	0.5
LHV (kJ/kg)	16250	28950	25000
m_O (kg O_2/kg coal)	1.2	2.2	2.0

[(1)]Oxygen to balance

Caption of figures

Fig. 1. Schematic layout of the CLOU system.

Fig. 2. Equilibrium oxygen concentration over the CuO/Cu_2O system as a function of temperature.

Fig. 3. Effect of temperature (a) y_{O_2} = 0 vol.%, and (b) y_{O_2} = 1.5 vol.%, on the oxygen carrier reduction rate using N_2. Symbols, experimental data; continuous line, model predictions.

Fig. 4. Effect of oxygen concentration (vol.%) at 1273 K on the oxygen carrier reduction, using N_2+O_2 mixtures. Symbols, experimental data; continuous line, model predictions.

Fig. 5. Effect of (a) O_2 concentration (vol.%) at 1173 K and (b) temperature with a y_{O_2} = 21 vol.%, on the oxygen carrier oxidation. Symbols, experimental data; continuous line, model predictions.

Fig 6. Arrhenius plots to calculate global activation energy in Eq. (6): ●, reduction; ▲, oxidation; for the Cu60MgAl.

Fig. 7. Effect of the oxygen concentration in the reaction order of Eq. (7) for: (a) reduction; (b) oxidation.

Fig.8. Determination of N parameter using conversion data to calculate $(-\ln(1-X))^N$ vs time (Eq.(21)) at (a) 1273 K, 4 vol.% O_2 for reduction; and (b) 1173 K, 6 vol.% O_2 for oxidation.

Fig. 9. Temperature dependence of kinetic parameters for Cu60MgAl: kinetic constant for oxygen uncoupling (●); kinetic constant for oxidation (▲); and adsorption parameter *c* for reduction (■).

Fig. 10. Determination of (a) *n* and *c* parameters using Eq. (23) for reduction; and (b) *n* parameter using Eq. (30) for oxidation reactions.

Fig. 11. Minimum solids inventories per MW_{th}: fuel reactor (- - -), air reactor (- ·- ·-); and specific circulation rate of solids (——) using a lignite as a function of the variation of the oxygen carrier conversion between the fuel and air reactors. T = 1223 K. Solids flux hydrodynamic limit (·····) also shown.

Fig. 12. (a) O_2 concentration at the fuel reactor outlet and (b) CO_2 capture efficiency as a function of the variation of oxygen carrier conversion in the fuel reactor using lignite as fuel and different solids inventories in the fuel reactor: 1500(——), 500 (·····), 250 (---) and 150 (-·-) kg/MW_{th}. T_{FR} = 1223 K, $\eta_{CSS} = 0$.

Fig. 13. (a) O_2 concentration at the fuel reactor outlet and (b) CO_2 capture efficiency, as a function of the fuel reactor inventory for three different coals: HRB (——), lignite (····), LVB (-----),T_{FR} = 1223 K, η_{CCS} = 0%, ΔX_{OC} = 0.7. LVB with a $\eta_{CSS} = 90\%$ also shown (-·-). Experimental points obtained in the 1.5 kW_{th} continuous unit for CLOU process: HRB (▼) [8], lignite (●), LVB (▲) [10].

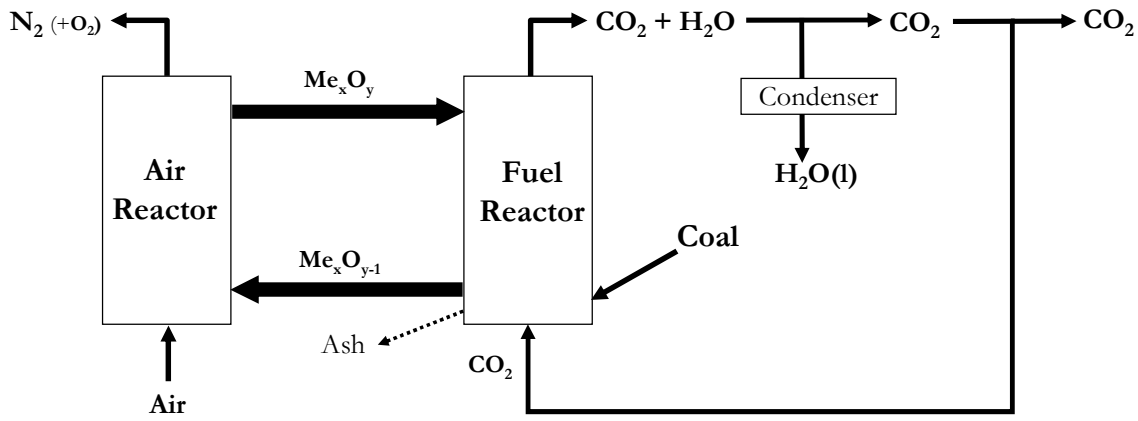

Fig. 1. Schematic layout of the CLOU system.

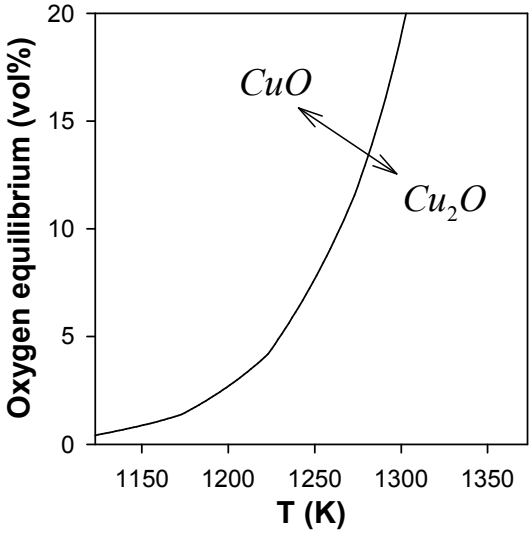

Fig. 2. Equilibrium oxygen concentration over the CuO/Cu_2O system as a function of temperature.

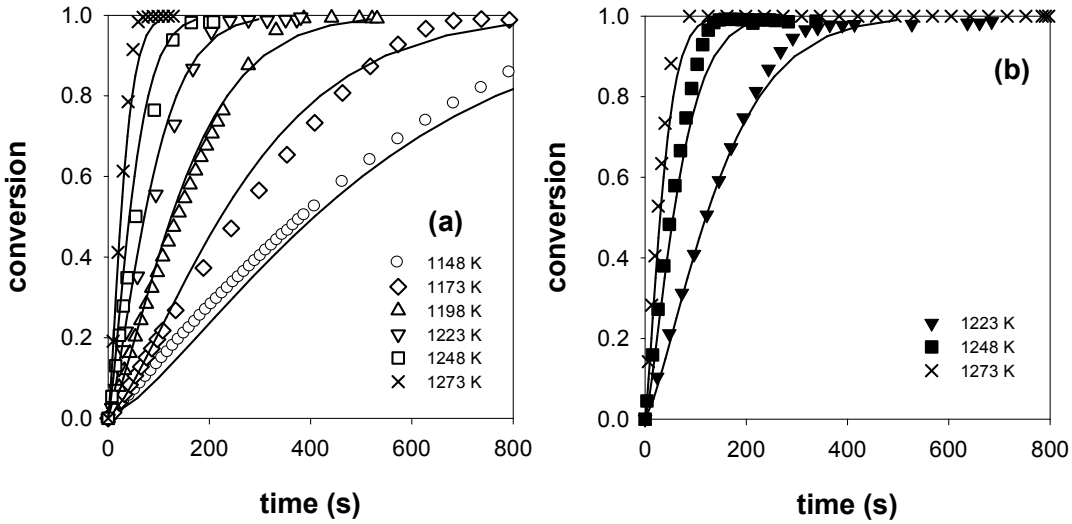

Fig. 3. Effect of temperature (a) y_{O_2} = 0 vol. %, and (b) y_{O_2} = 1.5 vol. %, on the oxygen carrier reduction rate using N_2. Symbols, experimental data; continuous line, model predictions.

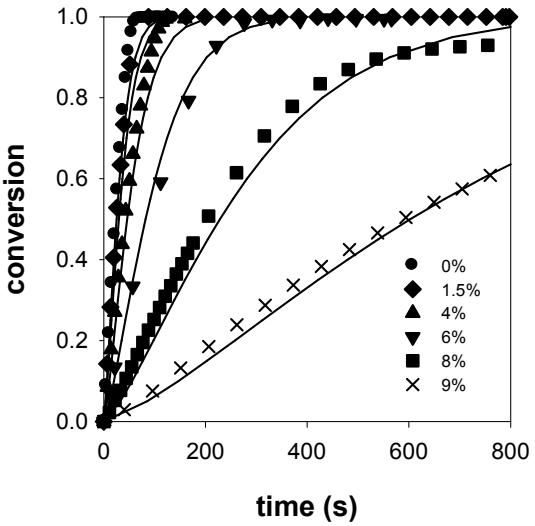

Fig. 4. Effect of oxygen concentration (vol.%) at 1273 K on the oxygen carrier reduction, using N_2+O_2 mixtures. Symbols, experimental data; continuous line, model predictions.

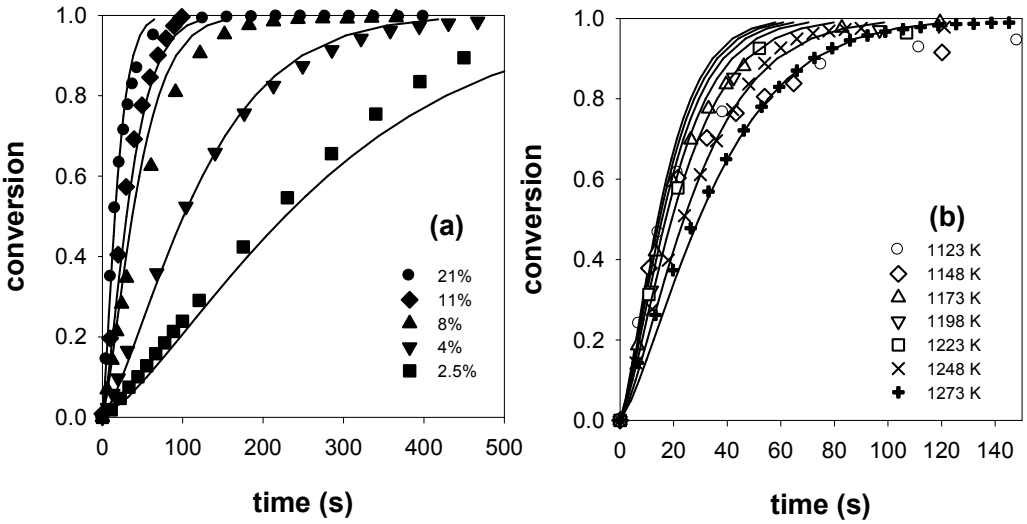

Fig. 5. Effect of (a) O_2 concentration (vol.%) at 1173 K and (b) temperature with a y_{O_2} = 21 vol.%, on the oxygen carrier oxidation. Symbols, experimental data; continuous line, model predictions.

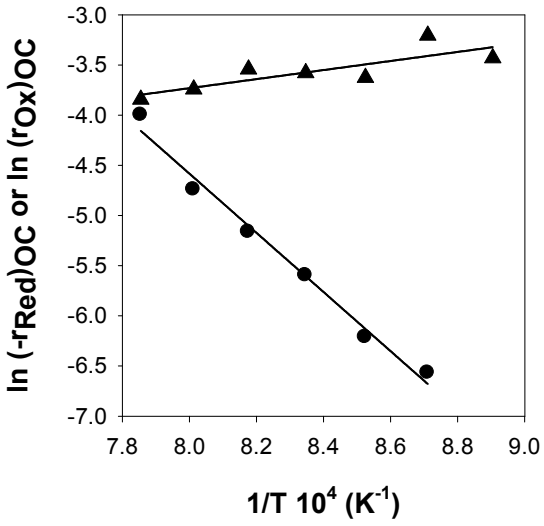

Fig 6. Arrhenius plots to calculate global activation energy in Eq. (6): ●, reduction; ▲, oxidation; for the Cu60MgAl.

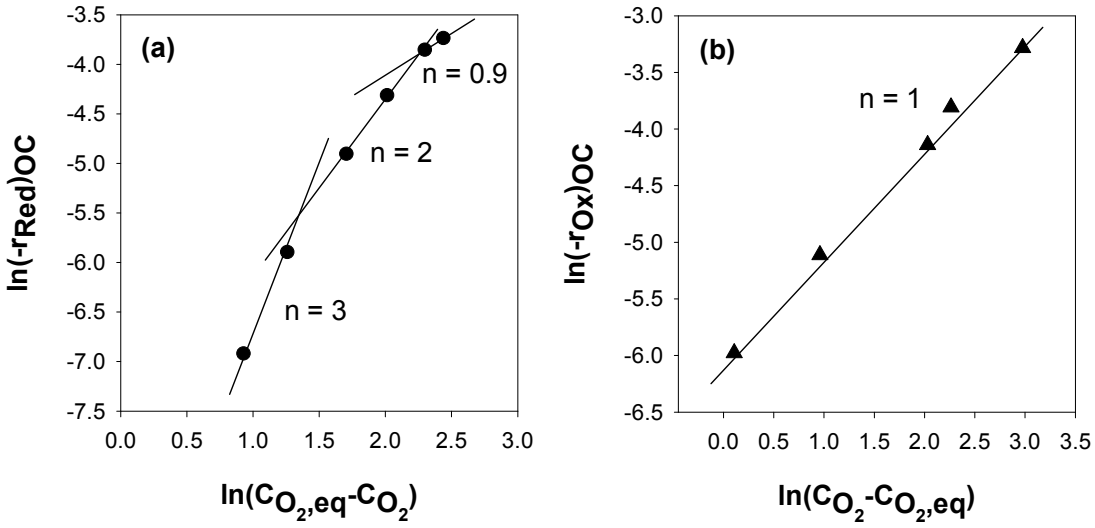

Fig. 7. Effect of the oxygen concentration in the reaction order of Eq. (7) for: (a) reduction; (b) oxidation.

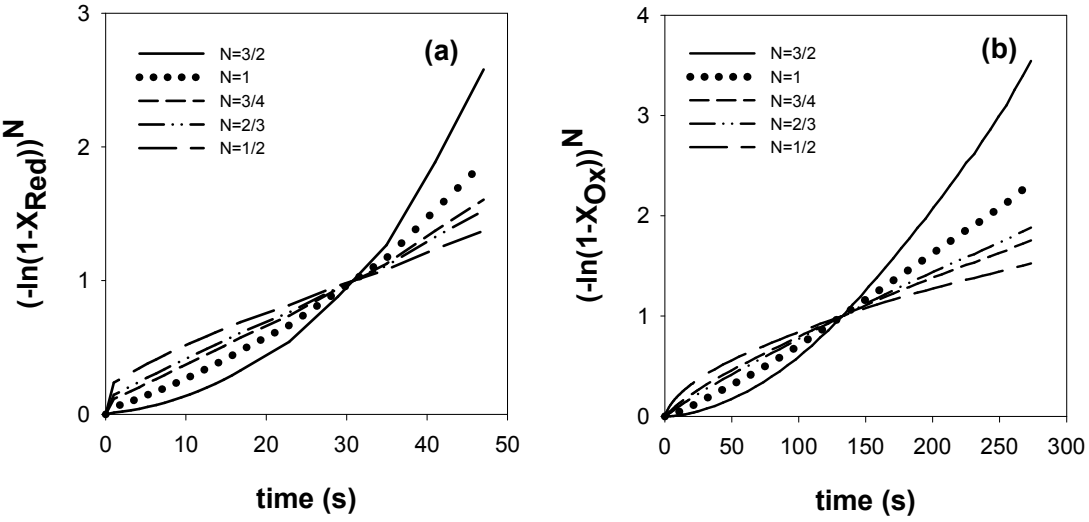

Fig.8. Determination of N parameter using conversion data to calculate $(-\ln(1-X))^N$ vs time (Eq.(21)) at (a) 1273 K, 4 vol.% O_2 for reduction; and (b) 1173 K, 6 vol.% O_2 for oxidation.

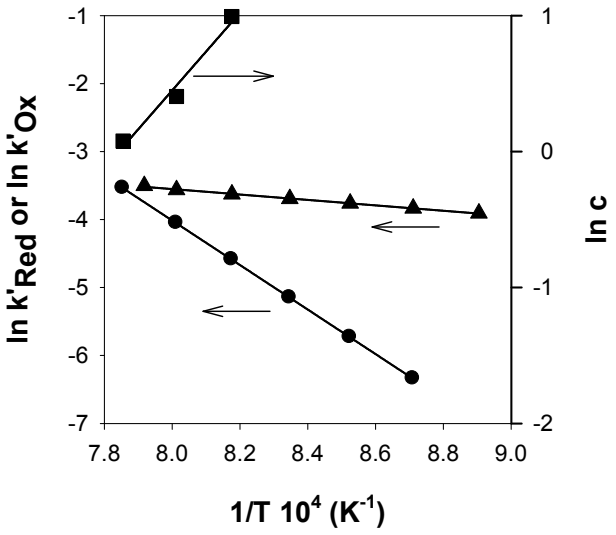

Fig. 9. Temperature dependence of kinetic parameters for Cu60MgAl: kinetic constant for oxygen uncoupling (●); kinetic constant for oxidation (▲); and adsorption parameter *c* for reduction (■).

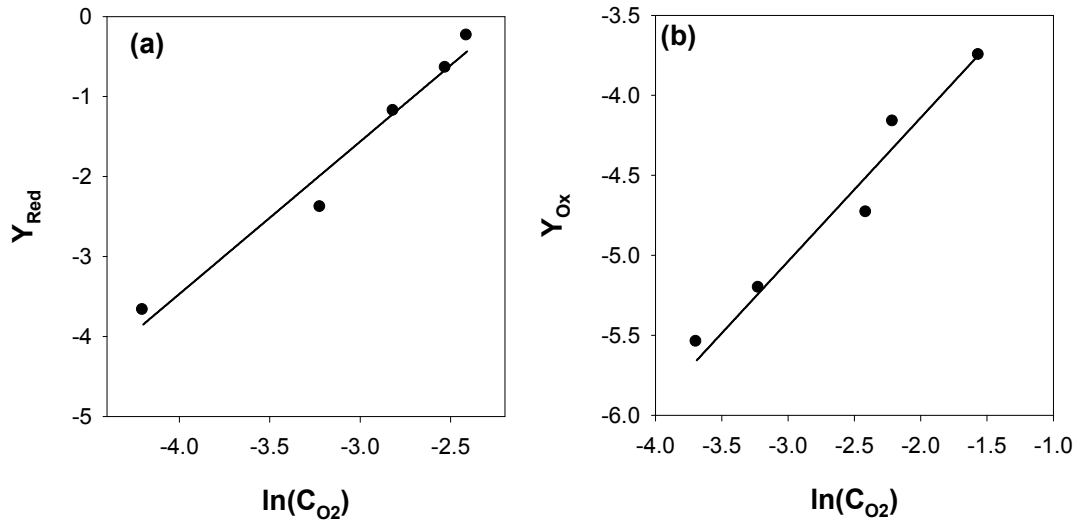

Fig. 10. Determination of (a) *n* and *c* parameters using Eq. (23) for reduction; and (b) *n* parameter using Eq. (30) for oxidation reactions.

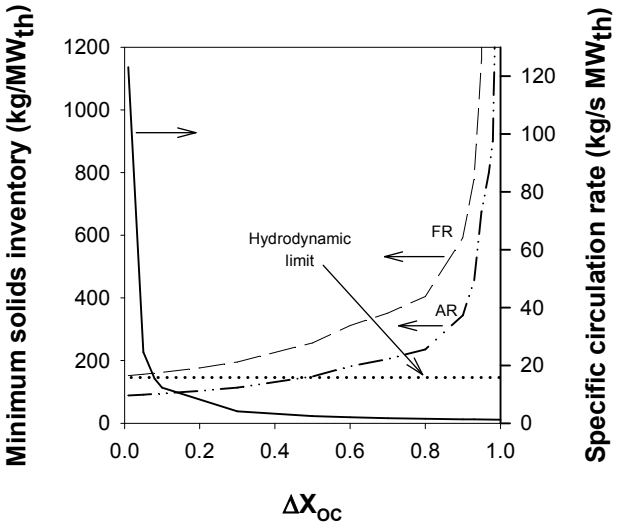

Fig. 11. Minimum solids inventories per MW_{th}: fuel reactor (- - -), air reactor (- ·- ·-); and specific circulation rate of solids (——) using a lignite as a function of the variation of the oxygen carrier conversion between the fuel and air reactors. T = 1223 K. Solids flux hydrodynamic limit (·····) also shown.

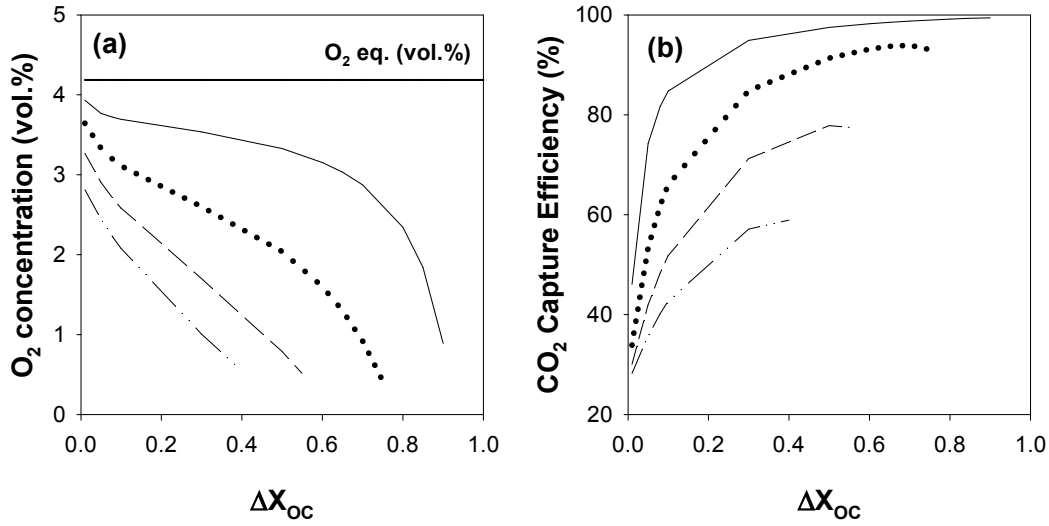

Fig. 12. (a) O_2 concentration at the fuel reactor outlet and (b) CO_2 capture efficiency as a function of the variation of oxygen carrier conversion in the fuel reactor using lignite as fuel and different solids inventories in the fuel reactor: 1500(——), 500 (·····), 250 (---) and 150 (-··-) kg/MW_{th}. T_{FR} = 1223 K, $\eta_{CSS} = 0$.

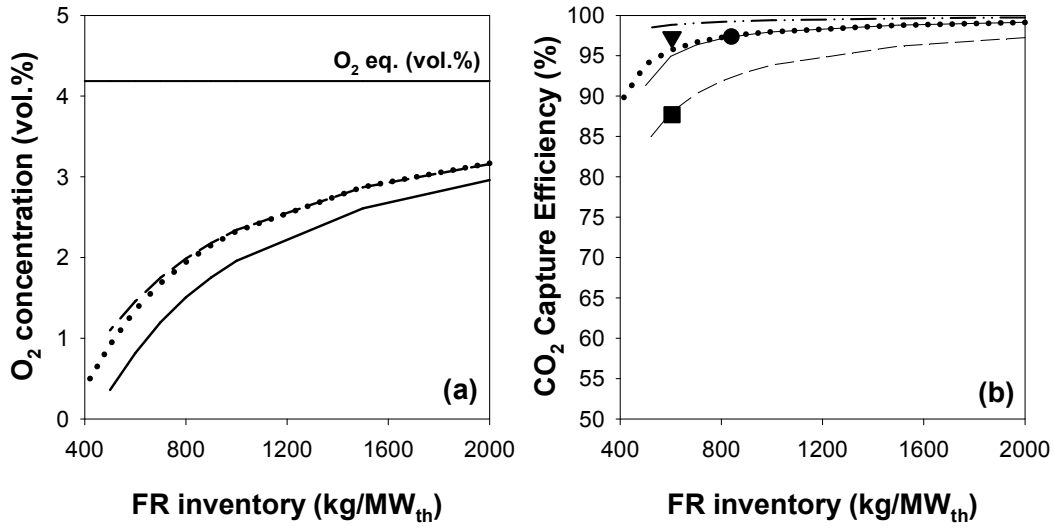

Fig. 13. (a) O_2 concentration at the fuel reactor outlet and (b) CO_2 capture efficiency, as a function of the fuel reactor inventory for three different coals: HRB (——), lignite (····), LVB (-----),T_{FR} = 1223 K, η_{CCS} = 0%, ΔX_{OC} = 0.7. LVB with a η_{CSS} = 90% also shown (-··-). Experimental points obtained in the 1.5 kW_{th} continuous unit for CLOU process: HRB (▼) [8], lignite (●), LVB (▲) [10].